doi:10.26443/seismica.v5i1.1839

Focal mechanisms in the southeastern South Island of Aotearoa New Zealand indicate scale-dependent partitioning of transpressional strain

Jack N. Williams * † [1,2], **Donna Eberhart-Phillips** [2], **Sandra Bourguignon** [3], **Mark W. Stirling** [1], **Martin Reyners** [3], **Phaedra Upton** [3]

[1]Department of Geology, University of Otago, Dunedin, New Zealand, [2]Earth Sciences New Zealand, Dunedin, New Zealand, [3]Earth Sciences New Zealand, Lower Hutt, New Zealand

Author contributions: *Conceptualization*: Jack N. Williams, Donna Eberhart-Phillips, Mark W. Stirling. *Formal Analysis*: Jack N. Williams, Donna Eberhart-Phillips, Sandra Bourguignon, Martin Reyners. *Funding Acquisition*: Mark W. Stirling. *Writing - Original draft*: Jack N. Williams. *Writing - Reviewing & Editing*: All authors.

Abstract The classic Andersonian model of faulting is difficult to apply to plate boundaries with oblique motion, as displacement is accommodated across oblique-slip faults, or it is partitioned into distinct strike-slip and dip-slip faults. Here, we investigate how faults accommodate oblique plate motion by using the focal mechanism solutions of 126 M_{Lv} 1.3-4.3 earthquakes in the transpressional southeastern South Island of Aotearoa New Zealand. Focal mechanisms were assigned an *A-D* quality, and of the 91 *C* or better quality solutions, 57 are strike-slip. In addition, when incorporated into a stress inversion, these focal mechanisms indicate a strike-slip stress state with an WNW-trending maximum principal compressive stress. By contrast, constraints on active crustal-scale faulting from the New Zealand Community Fault Model indicate reverse faulting in this region. A high stress shape ratio can partly account for the coexistence of reverse and strike-slip faults. However, we also propose that the focal mechanisms are typically sampling slip on optimally-oriented small-scale faults in intact crust, while the larger magnitude reverse faulting reflects local stress rotations within pre-existing faults and shear zones in the southeastern South Island. Our study therefore demonstrates how inherited structures influence the scale and orientation of faults onto which transpressional strain is partitioned.

Production Editor: Yen Joe Tan
Handling Editor: Robert Skoumal
Copy & Layout Editor: Anna M. Ledeczi

Signed reviewer(s): Mojtaba Rajabi

Received: July 10 2025
Accepted: December 16 2025
Published: January 19 2026

Non-technical summary When earthquakes occur, they release seismic waves. Since the motion within these waves has a predictable symmetry around the earthquake's causative fault, we can use seismic wave recordings to constrain the fault's orientation and slip sense. This information is represented using an earthquake 'focal mechanism.' In this study, we derived 126 focal mechanisms from small (M 1.3-4.3) earthquakes in the southeastern South Island of New Zealand, where the Australian and Pacific plates are moving through a combination of collision and horizontal lateral movement. However, the earthquake focal mechanisms we recorded generally indicate horizontal lateral movement. By contrast, large-scale faults in this region indicate convergence. From these observations, we suggest there is a scale dependence for how Australian-Pacific plate motion is being accommodated in the southeastern South Island, with lateral and convergence motions being accommodated in small and large earthquakes respectively.

1 Introduction

Our understanding of the relationship between fault orientations and stress states in the Earth's crust has a wide range of utilities for evaluating current and past crustal dynamics (Mercier et al., 1987; Hardebeck and Hauksson, 2001; Lanari et al., 2020), fluid flow (Barton and Zoback, 1992; Sibson, 1994; Ferrill et al., 2019), and seismic hazard (Morris et al., 1996; López, 2012; Yukutake et al., 2015; Williams et al., 2019). In isotropic crust undergoing plane strain, crustal stresses can be conveniently divided into 'Andersonian' normal, reverse, or strike-slip stress states, each of which has a predictable set of optimally-oriented conjugate faults (Anderson, 1905; Lisle et al., 2006; Célérier, 2008; Fossen, 2020). However, these predictions cannot be easily applied to regions experiencing transpressional or transtensional strain. Instead, these region's accommodate plate motion across oblique-slip faults or by the partitioning of strain into its pure and simple shear components (e.g., Sanderson and Marchini, 1984; Lettis and Hanson, 1991; Teyssier et al., 1995; Jones and Tanner, 1995; Dewey et al., 1998; Tamas et al., 2021; Zhang et al., 2025).

Earthquake focal mechanisms are a particularly useful tool for evaluating how transpressional and transtensional strain is released, as they provide in-situ information about fault orientations and kinematics. Furthermore, assuming that the maximum resolved shear stress acting on the fault plane is paral-

*Corresponding author: williams@lettisci.com
†Present address: Lettis Consultants International, Inc., Concord, CA, United States

lel to fault slip, focal mechanisms can be used to derive and map the crust's principal stresses orientations and relative magnitudes (e.g., Michael, 1984; Vavryčuk, 2014; Heidbach et al., 2018; Martínez-Garzón et al., 2016). However, focal mechanisms and stress states can be challenging to interpret in regions where strain is partitioned, as this implies small-scale switching of the principal strain and stress axes (Jones and Tanner, 1995; Abercrombie et al., 2000; Sibson et al., 2012; Kim et al., 2023). This can be further complicated in regions where the crust contains pre-existing faults and fabrics that can reactivate as unfavorably oriented oblique-slip faults (Lanari et al., 2020; Tamas et al., 2021) or that can locally rotate the principal stress axes (e.g., Twiss and Unruh, 1998; Faulkner et al., 2006; Morley, 2010; Williams et al., 2019).

In this study, we evaluate how oblique plate motion is accommodated between the Australian and Pacific plates on the southeastern South Island of Aotearoa New Zealand. In doing so, we explore an apparent contradiction between previous studies from in and around this region, which indicate a strike-slip stress state (e.g., Townend et al., 2012; Warren-Smith et al., 2017a,b; Holbek et al., 2020), and the surface expression of its active faults, which is comprised of a dominant set of NE-striking reverse faults and subordinate NW-striking reverse faults (Barrell, 2016, 2019; Seebeck et al., 2024). To do this, we resolve a new set of focal mechanisms for the southeastern South Island from temporary seismic array data (Reyners et al., 2017; Williams et al., 2025b), and from which we propose a model for scale-dependent release of transpressional strain.

2 Southeastern South Island seismotectonic setting

Within the South Island of Aotearoa New Zealand, the Pacific and Australian plates are obliquely converging along an ENE-trending azimuth at 35-40 mm/yr (Fig. 1; DeMets et al., 2010). In the southern South Island, the majority (∼70-90%) of this plate motion is accommodated to the west through dextral strike-slip on the Alpine Fault's southern section and convergence across the Puysegur Subduction Zone (Norris et al., 1990; Norris and Cooper, 2001; Barnes, 2009; Barth et al., 2014). Further east, is a ∼100-200 km wide low strain rate region that extends from the eastern edge of the Southern Alps and Fiordland to the South Island's east coast, and which forms the basis of our study area (Fig. 1).

From considering borehole breakouts (Sibson et al., 2012), slickenside orientations on outcrop-scale fault networks (Holbek et al., 2020), and first motion focal mechanisms (Balfour et al., 2005; Townend et al., 2012; Warren-Smith et al., 2017a,b; Matsuno et al., 2022), the stress tensor across the South Island is characterized by a strike-slip stress state (vertical stress, σ_v, = the intermediate principal compressive stress, σ_2) with a sub-horizontal ESE-trending maximum principal stress (σ_1). There are, however, nuances to this suggestion. Firstly, the stress state within our southeastern South Island study area is poorly constrained as low seismicity rates and the sparse coverage of the permanent GeoNet network (Eberhart-Phillips and Reyners, 2023; Warren-Smith et al., 2024) has made it challenging to obtain focal mechanisms from this region. More pertinently, while focal mechanisms indicate a strike-slip stress state, active fault maps and geodetic data indicate that deformation in the southeastern South Island is mainly accommodated on NE-striking reverse faults (Fig. 1a; e.g., Denys et al., 2016; Barrell, 2019, 2021; Seebeck et al., 2024). Because of these observations, the 2022 New Zealand National Seismic Hazard Model's (NZ NSHM 2022) distributed seismicity model considers both strike-slip and reverse mechanisms in this region (Thingbaijam et al., 2023).

In addition, the presence of the active NW-striking Waitaki and Waihemo reverse faults systems in north Otago/south Canterbury implies that σ_1 is locally rotated to a NE trend (Fig. 1a; Forsyth, 2002; Barrell et al., 2009; Upton et al., 2009; Gorman et al., 2013; Barrell, 2016, 2019; Seebeck et al., 2024). NE-oriented convergence around these faults is also supported by geodetic data (Denys et al., 2016; Haines and Wallace, 2020). NW-striking reverse faults are also mapped in south Otago and Southland (e.g., Tuapeka, Old Man, Clifton, and Hillfoot). Evidence of late Quaternary activity across these faults is equivocal (Fig. 1a; Hull and Stirling, 1992; Barrell, 2019), however, they have been active within southern New Zealand's current plate tectonic setting (i.e., since the late Miocene; Turnbull and Allibone, 2003; Cox and Sutherland, 2007; Barrell, 2021; Craw et al., 2022).

3 Methods

3.1 Southeastern South Island temporary seismic array deployments

We obtain focal mechanisms from earthquakes recorded by two temporary seismic deployments in the southeastern South Island, and which supplement the otherwise sparse (∼100 km station spacing) permanent GeoNet network in this region. The 'Otago' network (henceforth referred to as 'OtagoNet') was deployed between March 2014-April 2015, and consisted of a 40 station portable broadband network between southern Canterbury and eastern Southland (Fig. 1b; Reyners et al., 2017; Eberhart-Phillips et al., 2018, 2022b). For the Southland Otago Seismic Array (SOSA), 19 short period sensors were deployed from October 2022-October 2023 between eastern Southland and the edge of Fiordland (Fig. 1b; Williams et al., 2025b). This deployment was also supplemented by an ongoing temporary network in Fiordland (Fiord22; Eberhart-Phillips et al., 2023). Detected events were located with Simul2023 (Thurber and Eberhart-Phillips, 1999; Eberhart-Phillips et al., 2024) using the nzwide 3-D velocity model (Eberhart-Phillips et al., 2022a). Further details about these deployments, and how events were located, can be found in Reyners et al. (2017), Eberhart-Phillips et al. (2022b), and Williams et al. (2025b).

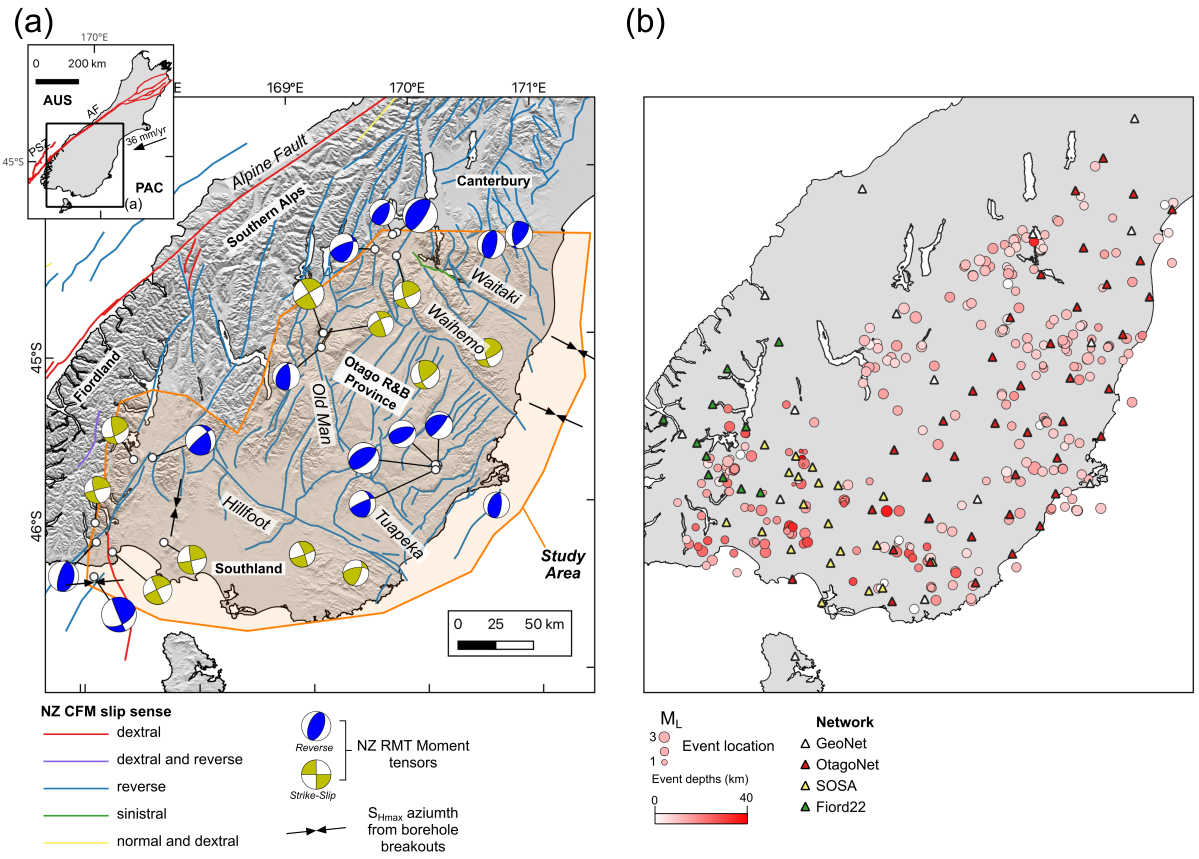

Figure 1 (a) Seismotectonic setting of the southeastern South Island of New Zealand as indicated by the distribution and kinematics of faults in the New Zealand Community Fault Model (NZ CFM; Seebeck et al., 2022, 2024), beach ball plots for events in the GeoNet regional moment tensor (RMT) catalog (2004-2025; Ristau, 2013), and the azimuth of the maximum horizontal stress (azS_{Hmax}) from borehole breakouts (as compiled in the World Stress Map; Heidbach et al., 2018). Inset, motion (DeMets et al., 2010) and principal structures between the Australian (AUS) and Pacific (PAC) plates in the South Island; AF, Alpine Fault; PSZ, Puysegur subduction zone. Italicized text; fault names. (b) Network configurations and seismicity recorded by the OtagoNet (March 2014-April 2015; Reyners et al., 2017) and Southland Otago Seismic Array (SOSA, October 2022-October 2023; Williams et al., 2025b).

3.2 Focal mechanism determination

Focal mechanisms are derived from the OtagoNet and SOSA deployments for earthquakes that had ≥8 manually picked *P*-wave polarities (*npol*) on the vertical channel. A quality (0, 1, or 2) was assigned to the polarity based on the pick quality. Events with focal depths >40 km were excluded as these earthquakes are likely to be nucleating within subducted remnants of the Hikurangi Plateau (Reyners et al., 2011, 2017; Eberhart-Phillips et al., 2018). As such, the stresses these deep earthquakes are responding to are not necessarily mechanically coupled to this region's ~15 km (in Canterbury and Otago) to ~40 km (in Southland) thick seismogenic layer (Warren-Smith et al., 2017a; Eberhart-Phillips et al., 2022b; Williams et al., 2025b).

We constrained focal mechanisms from these events based on their *P*-wave polarities and *S*-wave/*P*-wave (*S*/*P*) amplitude ratios using the program HASH v1.2 (for HArdebeck & SHearer; Hardebeck and Shearer, 2002). A full description of HASH is provided in Hardebeck and Shearer (2002) and Hardebeck (2003), and the settings we use are included in Table 1. However, in summary, for a given event, HASH first performs a grid search to identify an 'acceptable' set of focal mechanisms where the weighted proportion of misfit *P*-wave polarities (*mfrac*) and *S*/*P* ratios are less than a given threshold. Here, we set the *mfrac* threshold so that it is the greater of: (1) the number of misfit polarities for the best-fit mechanism ($npol_\phi$) plus an additional *nextra* misfits, or (2) *ntotal*, which is defined as *npol* multiplied by the fraction of assumed bad polarities (*badfrac*, set here to 10%, Table 1). We adopt the default HASH settings so that *nextra* is half of *ntotal*.

The *S*/*P* ratio can also be used to filter mechanisms as *P*-wave amplitudes increase at stations that plot close to the mechanism's *P* and *T* axes on a source's focal sphere, whereas *S*-wave amplitudes are largest for stations that plot near the nodal planes (Hardebeck, 2003; Yang et al., 2012). Notably, *S*/*P* ratios can increase the number of observations for constraining the focal mechanism, as they can use information from stations where there are travel-time picks but no polarity picks. Following Hardebeck (2003) and Yang et al. (2012), we measured *P* and *S* amplitudes from the vector norm of the maximum amplitudes on each of the three-component's waveforms after correcting for instrument response and filtering between 2-15 Hz. The minimum allowed *P*- and *S*-to-noise amplitude ratio, *ratmin*, is set

to 1 and 3 respectively (Table 1). A mechanism is accepted if the sum misfit between the mechanism's theoretical log(*S*/*P*) ratio and the observed log(*S*/*P*) ratio at each station (*qmis*) is less than a given threshold, which similar to polarity misfit threshold, is given by the greater of: (1) the sum of best-fit mechanism's *qmis* ($qmis_{\phi}$) and *qextra* or (2) *qtotal* (Table 1). In turn, *qtotal* is the assumed noise in the amplitude ratios (*qbadfrac*) multiplied by the number of (*S*/*P*) observations, and *qextra* is the larger of *qmisup* or half of *qtotal* (Table 1).

The process for finding acceptable mechanisms is then repeated in HASH using randomly changed 3-D raypaths for each event. The degree of these raypath perturbations are based on their azimuth and take-off angle error, which are calculated in Simul2023 from the event's hypocenter uncertainty. From the perturbed ray paths, additional acceptable mechanisms may be found. We perform this analysis following 30 trials, and where in each trial, the grid search for acceptable mechanisms is performed using a 5° grid spacing (*dang*, Table 1). If <10 accepted mechanisms are found, an additional search for solutions is made using 1.5∗*qmisup*.

To select a 'preferred' mechanism we find the five accepted mechanisms with the smallest *mfrac*, and from these, select the mechanism that has the smallest angular distance to the average P- and T-axis of all accepted mechanisms. In this way, our preferred solution balances the need to minimize solution misfits, and to ensure that it is not an outlier with respect to the accepted mechanisms. A quality *A*-*D* is also assigned to each focal mechanism based on: *mfrac*, the total number of polarity and *S*/*P* observations (*nobs*), the azimuthal gap (*gap*), the root-mean-square angular difference between the acceptable mechanism's P- and T-axes and the preferred mechanism's axes (*fm_rms*), and the proportion of acceptable mechanisms whose P- and T-axes are <30° from the preferred mechanism (*fm_prop*, Table 2, Fig. 2).

3.3 Stress inversion

Using the 91 *A*-*C* quality focal mechanisms derived from the OtagoNet and SOSA data, we conduct a stress inversion for the southeastern South Island using the program STRESSINVERSE (Vavryčuk, 2014). In addition, we incorporate 11 focal mechanisms reported by Warren-Smith et al. (2017a) that coincide with the north and western parts of our study area (Fig. 3), and that were obtained using the Central Otago Seismic Array (COSA) network between 2012-2013.

STRESSINVERSE solves for the orientations and relative magnitudes of the three principal stress by using a linear stress inversion method that recognizes that:

$$At = s \tag{1}$$

where A is a 3 × 5 matrix calculated from the fault normal, s is the slip vector on the fault, and t is the vector of stress components (Michael, 1984). Hence, for a set of m mechanisms, it is possible to extend Eq. 1 into 3 x m linear equations, and in which t can be solved using a linear least squares technique. Implicit in this approach is that: (1) the stress tensor is uniform within the region in which the focal mechanisms occur, (2) the slip vector is parallel to the direction of maximum resolved shear stress on the fault (i.e., the 'Wallace-Bott hypothesis'; Wallace, 1951; Bott, 1959), and (3) the trace of the stress tensor is zero (Michael, 1984).

A limitation of focal mechanism stress inversions is that the two nodal planes do not necessarily represent conjugate fault planes (Twiss and Unruh, 1998). Without prior knowledge of the earthquake's fault plane, it is therefore possible that the resulting stress tensor is influenced by the inversion incorrectly using the focal mechanism's auxiliary plane (Michael, 1987; Lund and Slunga, 1999; Martínez-Garzón et al., 2016). To address this, STRESSINVERSE first performs *N_realizations* iterations of the Michael (1984) stress inversion using randomly selected nodal planes. Then using the vector norm of these *N_realizations* stress tensors, the Mohr-Coulomb criterion is used to identify the nodal plane from each event that is most susceptible to failure (I), and this is selected as the fault plane during subsequent iterations (Vavryčuk, 2014). Here, I represents the ratio between the effective normal and shear stresses acting on a nodal plane relative to those on a fault that is optimally oriented in that stress state (Vavryčuk, 2014). To calculate I, we considered a range of fault's frictional strength estimates, μ, between 0.4-1.0 and at intervals of 0.05, and select the μ that results in the highest mean value of the focal mechanism's instability (I_{mean}). This nodal plane selection procedure is then repeated another *N_iterations* times using the optimum value for μ.

STRESSINVERSE considers focal mechanism uncertainty by adding noise, with an assumed mean deviation, to each mechanism's nodal plane orientations and rake. The stress inversion procedure is then repeated *N_noise_realizations* times using the randomly perturbed nodal planes (Vavryčuk, 2014). Here, we instead randomly select *N_noise_realizations* 'acceptable' mechanism that HASH returned for each event, and use these solutions to perform the stress inversions. We maintain the default values in STRESSINVERSE for *N_realizations* (10), *N_iterations* (6) and *N_noise_realizations* (100).

In addition, we weight focal mechanisms in STRESSINVERSE by the quality assigned to them using Table 2: w = 3 for *A*-quality, w = 2 for *B* quality, and w = 1 for *C*-quality. Kilb and Hardebeck (2006) recommend that only focal mechanisms with *fm_rms* <35° are used in stress inversions, and although our criteria for *C*-quality focal mechanisms is *fm_rms* <45° (Table 2), only 14 of the 91 OtagoNet and SOSA *C* or better quality focal mechanisms had *fm_rms* >30° and none had *fm_rms* >35°. We assign a nominal uncertainty of 15° to the strike, dip, and rake of the COSA focal mechanisms, and since they were derived using between 8-13 polarity observations (Warren-Smith et al., 2017a), they are assigned as *C* quality focal mechanisms.

To test if the stress state is uniform in the southeastern South Island, we subdivide the focal mechanisms using two approaches. In the first instance, focal mechanisms are grouped into three sub-regions based on NZ CFM fault orientations and crustal rheology (Fig. 3): (1) Southland, where there is a mixture of NE- and NW-

	Setting	Description	Value
Event selection	*npol*	Number of polarity observations	
	nspr	Number of *S*/*P* ratio observations	
	nobsmin	Minimum of*npol*+*nspr*	9
	delmax	Maximum allowed epicentral distance (km)	300
	mxpqual	maximum *P*-pick quality	2
Polarity misfits	*mfrac*	Weighted fraction misfit polarities	
	badfrac	Fraction of polarities assumed bad	0.1
	$npol_\phi$	Number of misfit polarities for best fitting mechanism	
	ntotal	Parameter for *mfrac* threshold	$npol * badfrac$
	nextra	Parameter for *mfrac* threshold	$ntotal * 0.5$
	mfrac threshold	Acceptable number of polarity errors	$max(npol_\phi + nextra, ntotal)$
Log *S*/*P* ratios	*ratmin*	Minimum allowed *P*-signal to noise ratio	1.0
	ratmin	Minimum allowed *S*-signal to noise ratio	3.0
	qmis	Sum misfit between mechanism's theoretical and observed log(*S*/*P* ratio)	
	qbadfrac	Assumed noise in *S*/*P* amplitude ratios in log10 scale	0.15
	$qmis_\phi$	*qmis* of best fit mechanism	
	qmisup	Limit for acceptable *S*/*P* amplitude ratio misfit	3
	qtotal	Parameter for *qmis* threshold	$nspr * qbadfrac$
	qextra	Parameter for *qmis* threshold	$max(qtotal * 0.5, qmisup)$
	qmis threshold	Acceptable log10(*S*/*P*) misfit	$max(qmis_\phi + qextra, qtotal)$
Grid Search	*dang*	Grid search angle focal mech (°)	5
	nmc	Number of trials	30
	maxout	Maximum returned focal mechanisms	500
	prob_max	Probability threshold for multiples	0.2

Table 1 Explanation and values of settings applied in HASH

Quality	*nobs*	*gap*	*mfrac*	*fm_prop*	*fm_rms*	*n* OtagoNet Events	*n* SOSA Events
A	≥40	≤140°	≤10%	≥90%	≤25°	3	3
B	≥25	≤210°	≤20%	≥60%	≤35°	15	19
C	≥10	≤270°	≤30%	≥50%	≤45°	44	7
D	all other events					34	1

Table 2 Criteria used to determine focal mechanism quality: *nobs*, number of polarity and *S*/*P* ratio observation; *gap*, azimuthal gap; *mfrac*, weighted fraction of misfit polarities; *fm_prop*, proportion of acceptable mechanisms with an angular distance <30° from the preferred mechanism; *fm_rms*, root-mean-square of the angular distance between the preferred and acceptable mechanisms. We also report the number of events for each quality level for the OtagoNet and SOSA data.

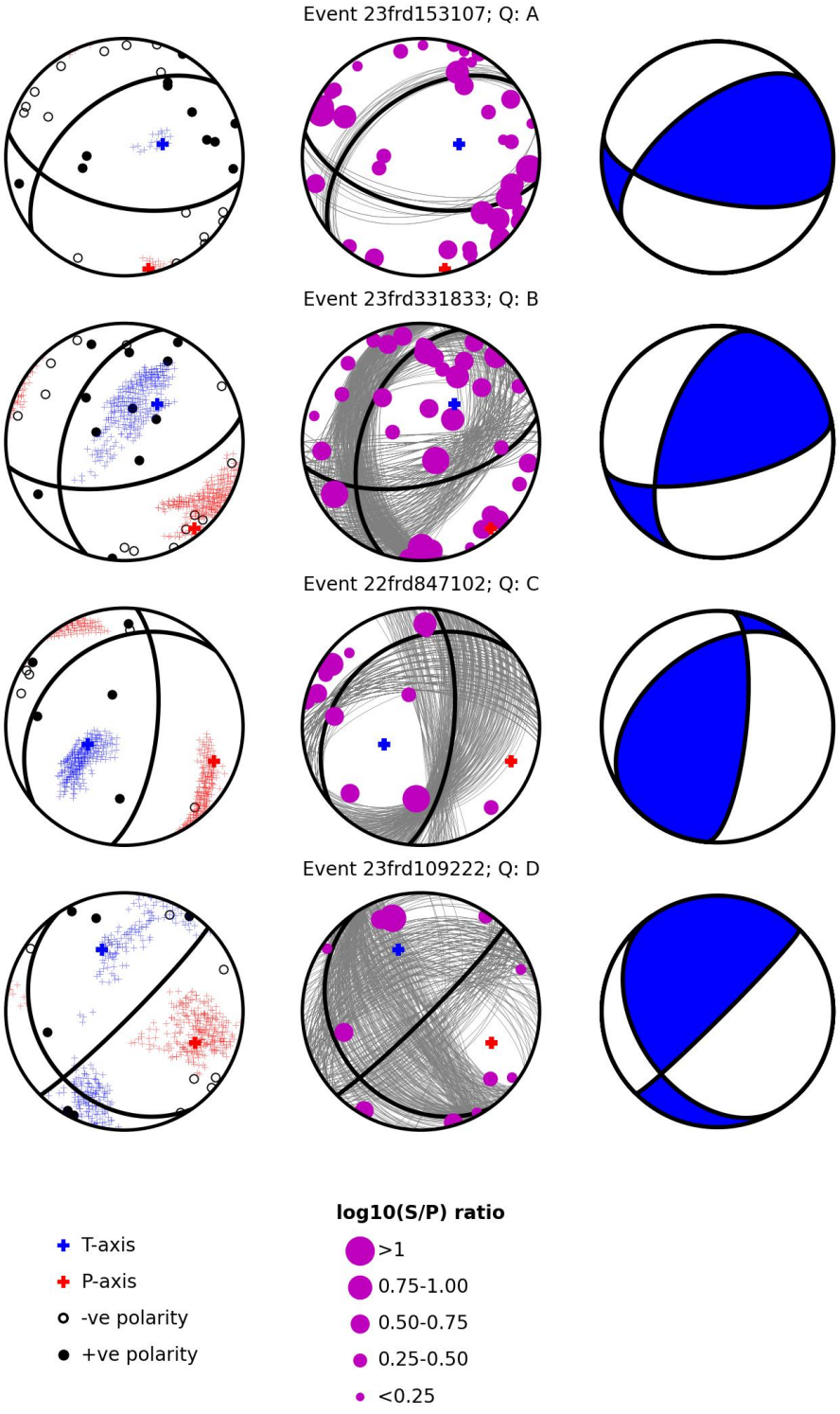

Figure 2 Examples of *A* to *D* quality focal mechanisms resolved from SOSA. For each event, the left plot indicates: the recording station's projection and first motion polarity, the preferred and accepted *P*- and *T*-axes, and the preferred nodal planes. In the center column, we show the *S*/*P* ratio at each recording station and the range of accepted nodal planes. Right column shows the event's preferred focal mechanism as a beach ball plot.

striking reverse faults, and the crust is composed of relatively strong and rigid mafic terranes that were accreted onto the Gondwana margin during the Mesozoic (Turnbull and Allibone, 2003; Eberhart-Phillips et al., 2022b; Williams et al., 2025b), (2) the Otago 'Range and Basin Province,' which is dominated by NE-striking reverse faults hosted in relatively weak quartzofelspathic Haast Schist (Turnbull, 2000; Norris, 2014; Eberhart-Phillips et al., 2018, 2022b), and (3) the Waitaki region, which lies at the transition between Haast Schist and relatively strong Rakaia Terrane derived greywacke, and is dominated by the NW-striking Waitaki and Waihemo reverse fault systems (Forsyth, 2002; Upton et al., 2009; Barrell, 2016).

In our second approach, we objectively group the focal mechanisms using a *k*-means algorithm (Hartigan and Wong, 1979; Martínez-Garzón et al., 2016; Warren-Smith et al., 2017b). This algorithm assigns earthquakes to clusters through an iterative approach that minimizes an error function between the earthquake locations and a predefined number of clusters. Given the 102 available focal mechanisms, and that the number of events in each cluster should be $\geq$30 (Martínez-Garzón et al., 2016), we tested groupings with two or three clusters. We then selected the grouping that returns the highest average silhouette coefficient (Rousseeuw, 1987; Martínez-Garzón et al., 2016), which in this instance, is the one with two clusters (scores are 0.55 and 0.51 for the groupings with two and three clusters respectively, Fig. S1).

We also conducted a stress inversion using the 25 solutions that are currently available for the southeastern South Island in the GeoNet Regional Moment Tensor (RMT) catalog (Fig. 1a; Ristau, 2013). These events occurred between 2004-2023 and had magnitudes M_W 3.5-4.7 (Fig. S2). To explore the RMT's uncertainty, we repeat these inversions *N_noise_realizations* times using fault planes that are randomly sampled from uniform distributions that are centered on the RMT solution's fault plane and bounded by nominal uncertainties of $\pm5°$, $\pm10°$, and $\pm15°$ for strike, dip, and rake respectively.

4 Results

4.1 Focal mechanisms

In total, we extract 96 and 30 focal mechanisms from M_{Lv} 1.14-4.3 events recorded by the OtagoNet and SOSA deployments respectively (see Williams et al., 2025a, for a full list). Focal mechanism qualities are typically *B* or *C* (Table 2). Overall, we resolve higher quality focal mechanisms from the SOSA data, which reflects that more polarity observations and *S*/*P* ratios were available for these events (average *nobs* is 22 and 89 for events from the OtagoNet and SOSA data respectively).

The focal mechanisms we resolve are predominantly strike-slip (*n*=74), with 35 and 17 reverse and normal focal mechanisms respectively. For comparison, if we only consider the 91 *A*-*C* quality solutions, the number of strike-slip, reverse, and normal focal mechanisms are 57, 26, and 8 respectively. It is ambiguous whether a strike-slip focal mechanism alone indicates dextral or sinistral faulting. However, following the nodal plane selection routine in STRESSINVERSE (Section 3.3), we infer that these strike-slip focal mechanisms can be distinguished into a set of subvertical E-striking dextral and SE-striking sinistral faults (Figs. 3 and S3). The angle between the average inferred dextral and sinistral plane is 54°, which is consistent with them representing a set of conjugate faults with Byerlee friction (Scholz and Choi, 2022). Relatively few focal mechanisms are resolved in southern Otago, which reflects that the seismic arrays recorded few events in this region (Fig. 1b).

4.2 Stress inversion results

Stress inversions that consider all available focal mechanisms in the southeastern South Island indicate a strike-slip stress state with a WNW-trending subhorizontal σ_1 (Table 3 and Fig. 4a). Once grouped by seismotectonic region, we find that the focal mechanisms in the Waitaki and Southland regions also indicate a strike-slip stress state with a WNW-trending σ_1 (Table 3 and Fig. 4b&d).

A reverse fault stress state is obtained from the Otago Range and Basin focal mechanisms (σ_v is equivalent to the minimum principal stress, σ_3); however: (1) the WNW trending σ_1 is the same as other regions, and (2) 43 out of the 100 *N_noise_realizations* inversions favor a strike-slip stress state (i.e., σ_2 plunge $>\sigma_3$ plunge, Fig. 4c). Indeed, 16/26 focal mechanisms in this region are strike-slip. We therefore suggest that it is equivocal from these stress inversions whether this region is under a reverse or strike-slip stress regime.

By alternatively grouping the focal mechanisms using a *k*-means clustering algorithm, we find similar stress states to the complete focal mechanism dataset (Table 3 and Fig. S4). The principal stress orientations for Cluster 2 are similar to those indicated for the Southland region (compare Figs. S4b and 4c). This reflects that Clusters 1 and 2 are divided by the region in southern Otago with relatively few focal mechanisms, and so the latter's spatial extent is similar to the Southland region (compare Figs. 3 and S1).

A reverse fault stress state with a gently plunging WNW trending σ_1 is obtained from the southeastern South Island's RMT solutions (Fig. 4e and Table 3). However, there is high uncertainty in the plunge of σ_2 and σ_3. In all inversions, the stress shape ratio ($R = \sigma_1 - \sigma_2/\sigma_1 - \sigma_3$) is $\geq$0.72 (Table 3, Figs. S5 and S6).

To examine the influence of STRESSINVERSE's procedure of using instability, *I*, to iteratively select nodal planes, we compare the stress tensor derived in the final iteration with that obtained by randomly selecting nodal planes. The average instability of focal mechanisms, I_{mean}, in these two inversions are 0.93 and 0.73 (Table 'ref_instability_info' in at Williams et al. (2025a)). Our comparison indicates that there is little difference in the principal stress orientations obtained from these two inversions (Table 3). However, *R* is significantly higher in the final iteration's stress tensor (0.74 vs 0.94). Hence, using *I* to iteratively selecting nodal planes in stress inversions primarily influences the stress shape ratio only (Michael, 1987; Vavryčuk, 2014; Martínez-Garzón et al., 2016).

5 Discussion

5.1 The stress state within the southeastern South Island

From considering all available focal mechanisms derived from the OtagoNet, SOSA, and COSA deployments, we infer a strike-slip stress state in the southeastern South Island with a WNW trending σ_1 and stress shape ratio, *R*, slightly less than 1 (Fig. 4a, Table 3). Spatially subdividing the focal mechanisms does indicate

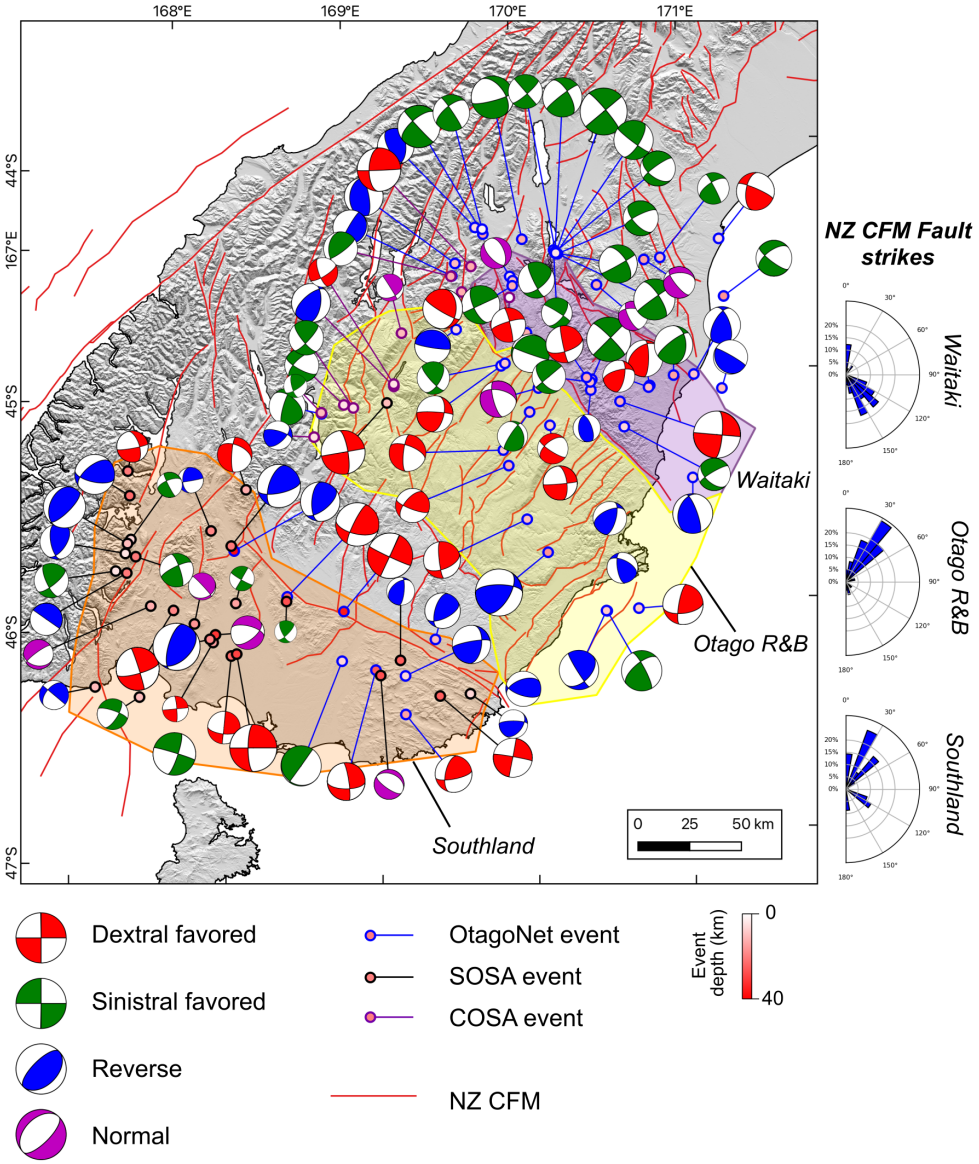

Figure 3 Beach ball plots showing the preferred first motion focal mechanisms derived from the OtagoNet and SOSA data. *D* quality events are excluded. We also show the 11 focal mechanisms constrained using the COSA (Warren-Smith et al., 2017a) that coincide with our study area east of the Southern Alps, and that are incorporated in our stress inversion. For strike-slip focal mechanisms, the beach balls are colored based on the kinematics of the nodal plane favored by STRESSINVERSE. Beach ball plot size scaled by event magnitude. Shading indicates the extent of regions from which focal mechanisms are selected for the Southland, Otago Range and Basin (R&B) and Waitaki stress inversions (Section 3.3). Side bar shows length-weighted rose plots for NZ CFM fault strikes in each of these regions.

that some small variations in the stress state may exist: an 8° clockwise rotation in the trend of σ_1 between the Otago Range & Basin province and Southland/Cluster 2 (Table 3), and a switch to reverse fault stress state in the Otago Range & Basin province. However, in the latter case, it is within our uncertainty that the stress state is strike-slip. More broadly, we highlight that in order for stress inversions to retrieve the correct stress orientations, the observed and theoretical fault slip vector orientations and symmetries should match (Twiss and Unruh, 1998). However, this assumption can break down, particularly in cases when there are limited data (n<50) and R is close to 1 (Martínez-Garzón et al., 2016). Hence, although we cannot exclude that the local variations in stress in Southland and Otago are real, our preferred interpretation is that the focal mechanisms indicate a broadly uniform stress state across the southeastern South Island.

If true, it indicates for the first time that this region's ESE trending maximum horizontal stress azimuth (azS_{HMax}) and strike-slip stress state is the same as inferred for elsewhere on the South Island (azS_{HMax} 115 ± 10°; Balfour et al., 2005; Townend et al., 2012; Sibson et al., 2012; Holt et al., 2013; Warren-Smith et al., 2017b; Matsuno et al., 2022). To the first order, this includes on the plate-bounding Alpine Fault itself (azS_{HMax} between 107-121°; Leitner et al., 2001; Boese et al., 2012; Michailos et al., 2020; Warren-Smith et al., 2022). Our

Data	Events	Stress State	σ_1 (plunge/ trend)	σ_2 (plunge/ trend)	σ_3 (plunge/ trend)	Stress Shape Ratio (R)	azS_{HMax}
All	102	strike-slip	01/296 (3)	77/204 (8)	13/026 (7)	0.94 (0.03)	116 (2)
All ref	102	strike-slip	01/116	77/209	13/026	0.74	116
Southland	36	strike-slip	06/124 (7)	63/225 (9)	27/031 (7)	0.76 (0.06)	124 (3)
Otago R&B	26	reverse	03/296 (8)	19/027 (43)	71/198 (43)	0.72 (0.1)	116 (5)
Waitaki	24	strike-slip	05/291 (8)	84/149 (11)	03/022 (7)	0.78 (0.07)	111 (3)
Cluster 1	62	strike-slip	03/110 (5)	87/321 (10)	02/200 (8)	0.82 (0.05)	110 (2)
Cluster 2	40	strike-slip	03/124 (7)	55/219 (9)	35/032 (7)	0.77 (0.07)	124 (3)
GeoNet RMT catalog	25	reverse	01/301 (4)	23/032 (21)	67/208 (20)	0.89 (0.06)	121 (3)

Table 3 Principal stress orientations, stress shape ratio (R), and azimuth of the maximum horizontal compressive stress (azS_{HMax}) obtained for the southeastern South Island from STRESSINVERSE. Numbers in brackets indicate uncertainties. For the principal stress orientations, uncertainties are represented by the average angular distance between the preferred stress orientations and those returned from the 100 *N_noise_realizations* inversions (see Section 3.3). The uncertainties of R and azS_{HMax} indicate one standard deviation of the *N_noise_realizations* inversions. Polygons used to divide focal mechanisms between the Southland, Otago Range and Basin(R&B), and, Waitaki regions are shown in Fig. 3. 'All ref' refers to the stress tensor returned from a stress inversion that incorporates randomly selected nodal planes.

interpretation also indicates that variations in NZ CFM fault orientations between Southland, the Otago Range and Basin province and the Waitaki (Fig. 3), nor differences in the rheology of basement terranes, correspond to regional azS_{HMax} rotations.

5.2 Controls on fault orientation and reactivation in the southeastern South Island

Collectively, the first motion focal mechanisms, regional moment tensors, and NZ CFM indicate that active reverse and strike-slip faults are present in the southeastern South Island of New Zealand. Elsewhere on the South Island, Sibson et al. (2012) used the example of the Canterbury Earthquake Sequence to propose that the coexistence of these fault types was facilitated by a R close to 1, as this implies that σ_2 and σ_3 can readily switch. Our stress inversions indicate that R >0.72 (Table 3, Fig. S5), and so this explanation can, at least partially, account for reverse and strike-slip faulting in the southeastern South Island too.

We highlight, however, that the first motion focal mechanisms typically indicate slip on E-W dextral or SE-NW sinistral fault planes (Figs. 5, 6, and S3), which given their M_{Lv} 1.14-4.3 magnitudes, correspond to events with a rupture diameter (r)∼0.04-0.5 km (assuming that the scaling between r and seismic moment, $M_0, = \frac{2}{7}\Delta\sigma r^3$, where $\Delta\sigma$ is stress drop (2.5 MPa) and that $log_{10}M_0 = 1.0M_L + 9.8$; Abercrombie, 1995, 1996; Scholz, 2019). Conversely, the NZ CFM, in conjunction with this region's paleoseismic record (e.g., Barrell, 2016, 2019; Williams et al., 2025c), indicates that surface rupturing ($M_W \geq$∼7.0, $r \geq$20 km) earthquakes in the southeastern South Island release strain on NE-, and subordinate NW-, striking reverse faults (Figs. 1a, 5d and 6b). This coexistence of relatively small-scale strike-slip and large-scale reverse faults in the southeastern South Island cannot be readily explained by a high R alone. Furthermore, a high R cannot account for the presence of active NE- and NW-striking reverse faults in this region, as this requires that σ_1 and σ_2 are similar in magnitude (Upton et al., 2009).

We therefore propose that the southeastern South Island focal mechanisms predominantly record slip on small-scale (r <∼0.5 km diameter) strike-slip faults in 'background' crust (Fig. 7a), and which in the context of Andersonian fault mechanics, are favorably-oriented for reactivation in this region's stress state (I_{mean} = 0.93, although we acknowledge there is some circularity here, as STRESSINVERSE will select the nodal plane that is more susceptible to failure). By contrast, we infer that the NZ CFM NE- and NW-striking reverse faults are currently active due to local stress state rotations within the damage zones of non-optimally oriented (I_{mean} for the southeastern South Island's NZ CFM faults = 0.80) Permian-Jurassic reverse faults and Cretaceous to mid-Cenozoic normal faults and shear zones in the southeastern South Island (Fig. 7a; e.g., Norris et al., 1990; Turnbull et al., 1993; Landis et al., 1999; Turnbull, 2000; Litchfield, 2001; Turnbull and Allibone, 2003; Norris, 2014; Mortimer et al., 2023).

In detail, two types of changes to the strike-slip stress state suggested by the focal mechanisms are required to explain the activation of non-optimally oriented reverse faults in the southeastern South Island. Firstly, σ_2 and σ_3 must locally rotate about a vertical plane orthogonal to σ_1 so that they switch positions, and NE-striking faults can activate as reverse faults (Koons, 1994; Enlow and Koons, 1998); the possibility of which is favored by the prolate stress ellipsoids we infer for this region (i.e., R is close to 1 and the magnitude of $\sigma_2 \sim \sigma_3$, Table 3). In addition, the activation of the NW striking Waitaki faults requires that σ_1 and σ_2 locally rotate about a horizontal axis (Upton et al., 2009). In both cases, these rotations can be driven by small changes in the horizontal or vertical shear stress (Enlow and Koons, 1998; Upton et al., 2009) that could conceivably occur in the relatively fractured and compliant damage zones of these faults (Twiss and Unruh, 1998; Faulkner et al., 2006; Gudmundsson et al., 2010; Ziegler et al., 2024).

Overall, a reverse fault stress state is obtained from 25 M_W 3.5-4.7 RMTs in the southeastern South Island (Fig. 4e and Table 3). However nearly half of the RMTs (11/25)

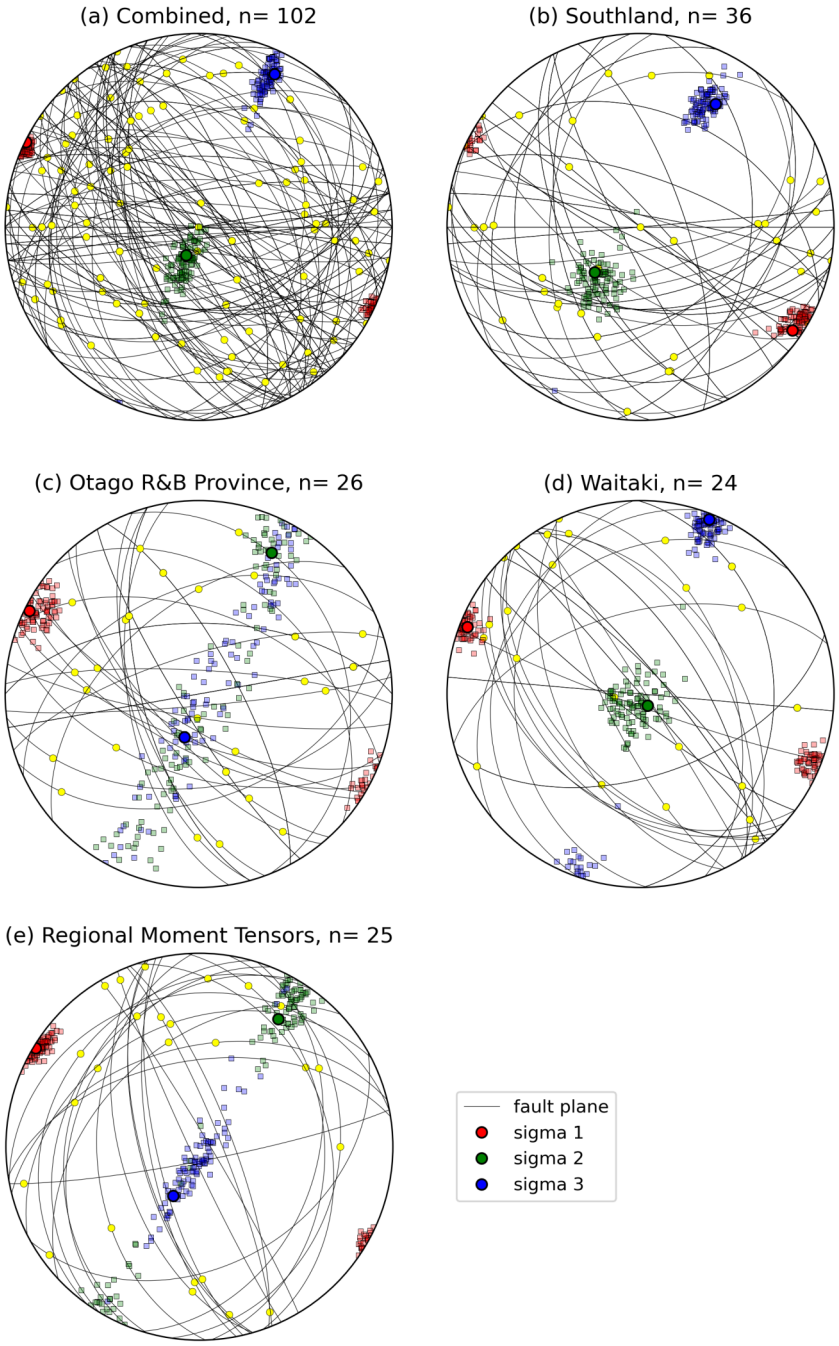

Figure 4 Lower hemisphere equal area stereonets depicting the orientations of the three principal stresses returned by STRESSINVERSE. Large red, green, and blue circle symbols represent the stress axes derived the 'preferred' focal mechanisms returned by HASH. Smaller colored squares represent the stress axes from 100 inversions that use randomly sampled 'accepted' focal mechanisms. The orientation and rake of each event's preferred nodal planes, as selected by STRESSINVERSE, are plotted as great circles with yellow squares. Plots are arranged to indicate the principle stresses from considering: (a) all available first motion focal mechanisms in the southeastern South Island, (b)-(d) focal mechanisms grouped by regions shown in Fig. 3, and (e) from events in the GeoNet Regional Moment Tensor catalog (Fig. 1a.)

are strike-slip events. We therefore suggest that the M_W 3.5-4.7 RMT events (r∼0.5-2.5 km) are within the transition between slip preferentially occurring on strike-slip faults in background crust or on non-optimally oriented reactivated reverse faults. We do not wish to explicitly assign a maximum magnitude to strike-slip earthquakes in the southeastern South Island. Nevertheless, we suggest that instead of assigning an equal weighting to reverse or strike-slip $4.95 \leq M_W \leq 8$ earthquakes for this region in the 2022 NZ NSHM distributed seismicity model (Thingbaijam et al., 2023), future updates should favor reverse fault earthquakes.

Our hypothesis of scale dependent fault kinematics cannot account for all of the southeastern South Island's faults. For example, 35/126 of the focal mechanisms indicate reverse faulting (Fig. 3). Although it is possible

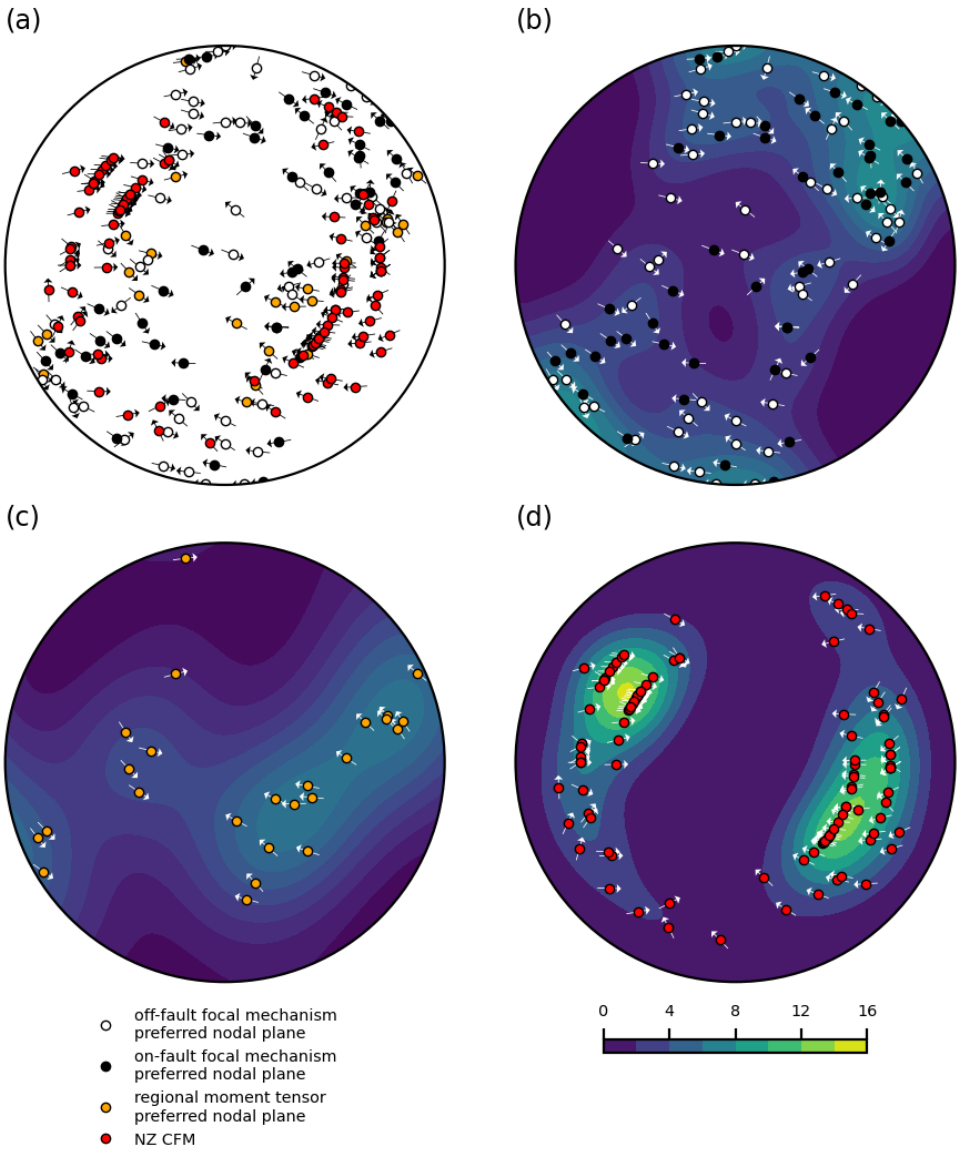

Figure 5 Tangent lineation plot for faults in the southeastern South Island from considering the first motion focal mechanism's (*C* quality or better), regional moment tensors,, and the NZ CFM (Seebeck et al., 2024). Plots follow the convention of Twiss and Unruh (1998), so that fault orientations are represented as poles-to-planes, and the arrows indicate slip direction of material outside the plotting hemisphere (i.e., the footwall for inclined faults and lower hemisphere projection). The first motion focal mechanisms are colored based on whether they are located <3 km from the down-dip projection of a fault in the NZ CFM geometric model (Seebeck et al., 2022). In (b)-(d) we plot each data subset and contour poles using a modified version of the Kamb method (Vollmer, 1995).

that these focal mechanisms represent events within the damage zones of NZ CFM reverse faults, distinguishing between focal mechanisms that are located <3 and >3 km of a fault in the NZ CFM geometrical model does not result in any discernible differences in stress states (Fig. 8). Holocene sinistral motion has also been documented on the crustal-scale Fern Gully Fault (Barrell, 2016). Indeed, many NZ CFM faults in the southeastern South Island lack *in situ* constraints on their kinematics, and so the inference that they are reverse dip-slip faults is often based on expert judgment. We highlight, however, that aside from the Fern Gully Fault, active fault studies do indicate dip-slip reverse faulting in this region (e.g., Barrell, 2016, 2019; Taylor-Silva et al., 2020; Griffin et al., 2022; van den Berg et al., 2024; Williams et al., 2024; Meyer et al., 2025), and geodetic data indicates that uniaxial compression is the predominant signature of elastic strain accumulation in the Otago Range and Basin province (Denys et al., 2016).

Instead of local stress rotations, an alternative explanation is that large-scale NE-striking reverse faults are activated in the southeastern South Island as they are frictionally weak (Smith et al., 2017), and under the Wallace-Bott hypothesis, would exhibit reverse fault slip in this region's strike-slip stress state anyway. While we do not entirely exclude this explanation, it would suggest that instead of activating as reverse faults, NW-striking faults in the Waitaki region should be predominantly sinistral. Indeed, our hypothesis for localized fault zone stress rotations is similar to numerical models that suggest these faults are activated due to a local switching between σ_1 and σ_2 at a rheologic transition

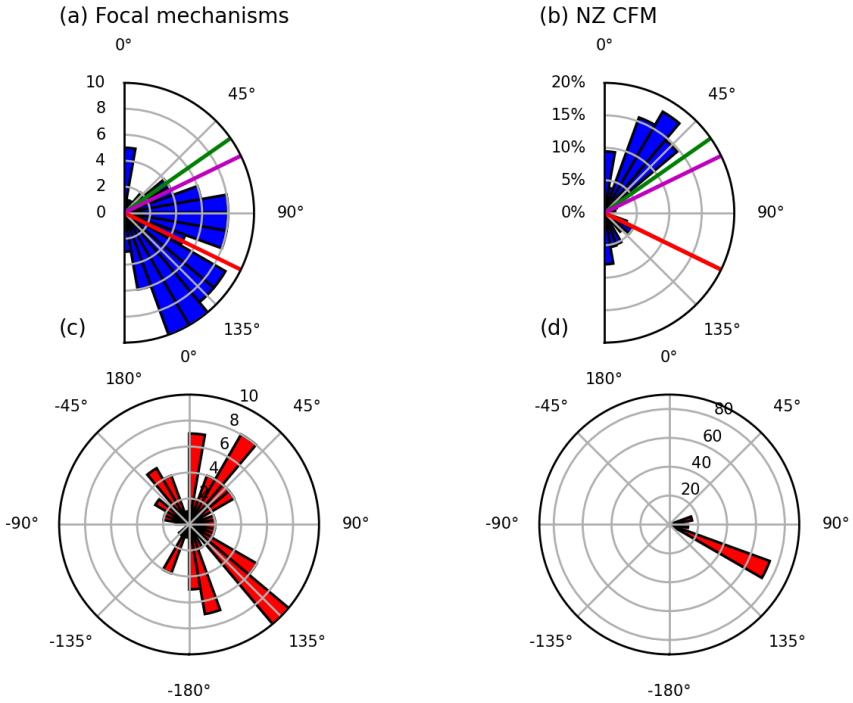

Figure 6 Rose plot indicating the distribution of fault strikes in the southeastern South Island from (a) the preferred nodal planes of OtagoNet, SOSA, and COSA first motion focal mechanisms (*C* quality or better) and (b) the NZ CFM. Strikes in (b) are weighted by fault length. Green, magenta, and red line indicates orientation of the plate motion margin (as indicated by the 055° striking Alpine Fault), plate motion vector (DeMets et al., 2010), and the 116° S_{Hmax} azimuth for the southeastern South Island (Table 3) respectively. (c&d) Equivalent to a&b but showing the distribution of rakes from (c) focal mechanisms and (d) NZ CFM faults.

between strong and weak lower crust in the Waitaki region (Upton et al., 2009, 2014). In detail, our stress inversions did not indicate a stress rotation within this region (Fig. 4d and Table 3); however, this does not preclude σ_1 and σ_2 switches occurring within individual fault zones due to a combination of pre-existing NW-striking faults (Forsyth, 2002; Gorman et al., 2013), and the reduced difference between the σ_1 and σ_2 at this region's rheologic transition (Upton et al., 2009).

5.3 Comparisons to slip partitioning in the South Island and beyond

Our observations of slip partitioning in the southeastern South Island are consistent with those from the central Southern Alps, where potentially active major faults indicate near pure-dip slip with an ESE shortening direction, while secondary faults and RMTs exhibit a combination of reverse and strike-slip faulting (Cox et al., 2012). In addition, the 1994 M_W 6.7 Arthur's Pass Earthquake is interpreted to have activated a NE-striking reverse fault within an overall strike-slip stress regime (Abercrombie et al., 2000; Robinson and McGinty, 2000). West of our study area, microseismicity is also dominated by strike-slip faulting (Warren-Smith et al., 2017a,b). However, slip is interpreted to preferentially occur on ENE-striking dextral planes, thereby indicating a rotation from E-striking dextral planes in our study area (Figs. 5) to ENE-striking as the Australian-Pacific plate boundary is approached.

To the north of our study area, it has been suggested that the E-striking dextral Greendale Fault, which ruptured during the M_W 7.1 2010 Darfield Earthquake, is reactivating a rheologic contrast where azS_{HMax} is rotated ~20° anticlockwise to an E-W trend (Browne et al., 2012; Holt et al., 2013; Ellis et al., 2016). Hence, although the Greendale Fault has been previously suggested to be favorably oriented to the regional stress state (Sibson et al., 2012), it may actually be consistent with our suggestion of localized stress rotations occurring within southeastern South Island's pre-existing faults.

The slip partitioning we describe is also part of a larger system of how transpressive Australian-Pacific plate motion is accommodated in the southern South Island. Broadly speaking, the majority of the plate-parallel motion is localized on the southern section of the NE-striking dextral Alpine Fault, and the plate-normal component is accommodated on parallel offshore thrusts, the Puysegur subduction zone, and the Otago Range & Basin's and Southland's reverse faults (Fig. 7b; Norris and Cooper, 2001; Barth et al., 2014; Barnes, 2009; Seebeck et al., 2024). This partitioning of transpressional strain onto sub-parallel thrusts and strike-slip faults is also observed in other oblique subduction zones (e.g., Webb and Anderson, 1998; McCaffrey, 2009; Schütt and Whipp, 2020), California (e.g., Mount and Suppe, 1988; Lettis and Hanson, 1991; Miller, 1998) and elsewhere (Lanari et al., 2020; Waldien et al., 2023). However, the southeastern South Island indicates additional nuances for how transpressional strain

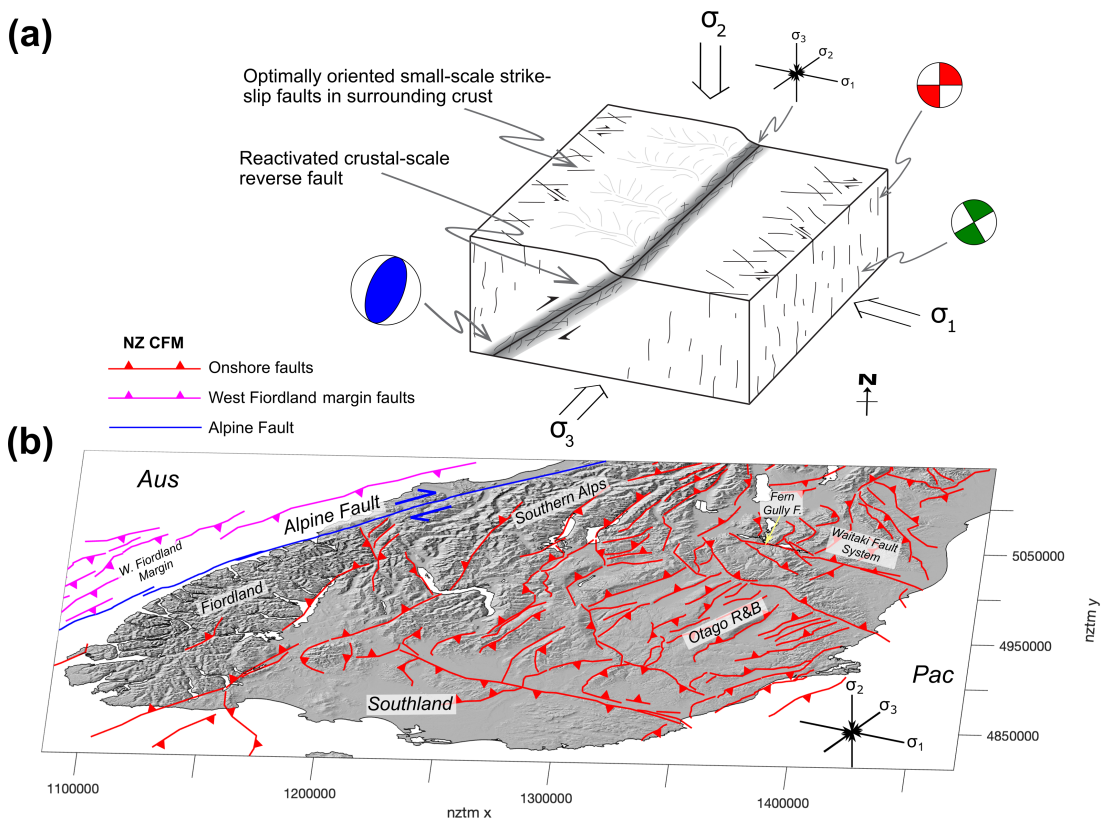

Figure 7 (a) Schematic representation of our model for scale dependent fault kinematics in the southeastern South Island. The first motion focal mechanisms predominantly sampled slip on small-scale (rupture radius 0.04-0.5 km) favorably oriented strike-slip faults. By contrast, the surface expressions of faulting in this region indicate slip on NE-striking reverse faults, and which we infer formed due to stress rotations within reactivated fault zones. (b) Oblique perspective of faulting across the Australian-Pacific plate boundary in the southern South Island, as indicated by the NZ CFM (Seebeck et al., 2024).

is partitioned in that: (1) slip partitioning is scale-dependent, (2) strike-slip faults are oblique to reverse faults and the plate boundary margin (Figs. 5 and 6), and (3) it highlights the role of stress rotations within pre-existing fault and shear zones during slip partitioning (Jones and Tanner, 1995; Waldien et al., 2023). Our observations of scale-dependent fault orientations bears similarities to those from Scholz and Choi (2022); however, instead of up-dip propagation of underlying viscous shear zones, we suggest that this scale dependence is driven by the reactivation of non-optimally oriented faults.

6 Conclusions

To examine how oblique motion between the Australian-Pacific plates is accommodated in the southeastern South Island of Aotearoa New Zealand, we used temporary seismic data to constrain focal mechanisms from 126 M_{Lv} 1.14-4.3 earthquakes. These focal mechanisms predominantly indicate slip on a conjugate set of E-striking dextral and NW-striking sinistral strike-slip fault planes with rupture diameters <∼0.5 km. A stress inversion conducted using these focal mechanisms also indicates a strike-slip stress state with an WNW-trending maximum principal compressive stress and stress shape ratio <∼1; a result consistent with stress inversions conducted elsewhere on the South Island.

Unlike the strike-slip faulting indicated by the first motion focal mechanisms, the New Zealand Community Fault Model (NZ CFM, fault lengths >10 km) implies that large magnitude surface rupturing events in the southeastern South Island activate NE, and subordinate NW, striking reverse faults. From these contrasting observations, we propose that the first motion focal mechanisms predominantly sample earthquakes on small-scale strike-slip faults that are favorably oriented for reactivation in this region's stress state. The larger-scale reverse faulting indicated by the NZ CFM reflects stress rotations and/or switches between the principal stress axes within reactivated faults and shear zones. If true, then the southeastern South Island highlights that pre-existing structures can lead to scale-dependent partitioning of transpressional strain on obliquely-oriented dip-slip and strike-slip faults.

Acknowledgements

The Southland Otago Seismic Array (SOSA) was supported by the Natural Hazard Commission Toka Tū Ake University Research Program project RCP023 'Seismic hazard of the southern South Island: the neglected provinces.' JW also acknowledges funding

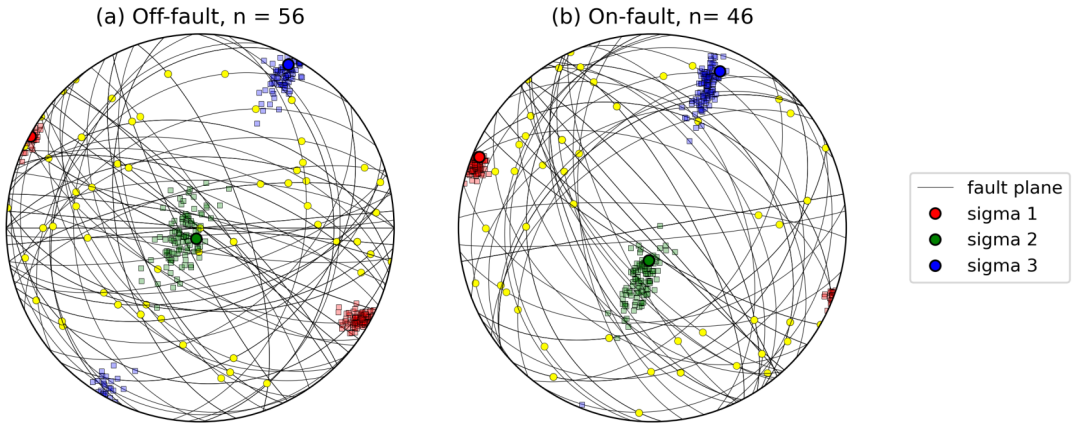

Figure 8 Orientation of the three principal compressive stresses for southeastern South Island focal mechanisms, once filtered for events that are located (a) >3 km or (b) <3 km from a fault in the NZ CFM (Seebeck et al., 2022). Figure follows convention of Fig 4, with smaller square symbols representing the stress axes from randomly sampled 'accepted' focal mechanisms, and the greater circles represent the orientation and rake of the preferred nodal plane selected by STRESSINVERSE. We highlight that this analysis does not consider uncertainty in the down-dip projection of NZ CFM faults, or that the stress rotations are occurring in zones <6 km wide (note that that a 1 km cut-off for 'on-fault' would result in only 12 'on-fault' focal mechanisms in our catalog).

from the Aotearoa New Zealand's Ministry of Business, Innovation and Employment (MBIE) through the Aotearoa New Zealand National Seismic Hazard Model Project (contract 110316). We thank the Australian National Research Facility for Earth Sounding (ANSIR, auscope.org.au/ansir) for providing equipment for the SOSA deployment, Luke Easterbrook-Clarke for help with figures. We are grateful to David Barrell for discussions about active faulting in the southeastern South Island, and John Ristau for his guidance on incorporation of the New Zealand Regional Moment Tensor Catalog into a stress inversion. This study also benefited from helpful editorial comments from Robert Skoumal and reviews by Mojtaba Rajabi and an anonymous reviewer.

Data and code availability

At Williams et al. (2025a), we have uploaded: supplementary figures S1-S6, a catalog for the 126 focal mechanisms resolved from the OtagoNet and SOSA deployments, focal mechanism plots for these events (following the template in Fig. 2), a catalog of the 11 focal mechanisms constrained from the COSA (Warren-Smith et al., 2017a) that are located within our study area, a RMT catalog for the southeastern South Island, and a list of the instability of the OtagoNet, SOSA, and COSA focal mechanisms in the stress tensors indicated by STRESSINVERSE (for events with quality greater than *C*).

Data from the OtagoNet and SOSA deployments are archived with the International Federation of Digital Seismograph Networks (FDSN) Web Service at Services at https://doi.org/10.7914/jr68-qq17 (Reyners, 2014) and https://doi.org/10.7914/SN/6K_2014 (Williams et al., 2022) respectively. The GeoNet regional moment tensor catalog was obtained from: https://github.com/GeoNet/data/tree/main/moment-tensor (date last accessed 28/02/2025) and the New Zealand Community Fault Model is available at: https://www.gns.cri.nz/data-and-resources/new-zealand-community-fault-model/ (date last accessed 02/04/2025).

The HASH v1.2 program is available at: https://www.usgs.gov/node/279393 (date last accessed 03/12/2024) and the STRESSINVERSE package (Vavryčuk, 2014) at: https://www.ig.cas.cz/en/stress-inverse/ (date last accessed 13/01/2025). Stereonets depicting the accepted mechanisms P- and T-axes and beach ball plots of the preferred mechanism are plotted using mplstereonet (https://mplstereonet.readthedocs.io/en/latest/index.html, date last accessed 04/12/2024) and ObsPy (https://docs.obspy.org, date last accessed 04/12/2024) respectively.

Competing interests

The authors declare they have no competing interests.

References

Abercrombie, R. E. Earthquake source scaling relationships from −1 to 5 ML using seismograms recorded at 2.5-km depth. *Journal of Geophysical Research: Solid Earth*, 100(B12):24015–24036, Dec. 1995. doi: 10.1029/95jb02397.

Abercrombie, R. E. The magnitude-frequency distribution of earthquakes recorded with deep seismometers at Cajon Pass, southern California. *Tectonophysics*, 261(1–3):1–7, Aug. 1996. doi: 10.1016/0040-1951(96)00052-2.

Abercrombie, R. E., Webb, T. H., Robinson, R., McGinty, P. J., Mori, J. J., and Beavan, R. J. The enigma of the Arthur's Pass, New Zealand, earthquake: 1. Reconciling a variety of data for an unusual earthquake sequence. *Journal of Geophysical Research: Solid Earth*, 105(B7):16119–16137, July 2000. doi: 10.1029/2000jb900008.

Anderson, E. M. The dynamics of faulting. *Transactions of the Edinburgh Geological Society*, 8(3):387–402, 1905.

Balfour, N. J., Savage, M. K., and Townend, J. Stress and crustal anisotropy in Marlborough, New Zealand: evidence for low fault strength and structure-controlled anisotropy. *Geophysical Journal International*, 163(3):1073–1086, Dec. 2005. doi: 10.1111/j.1365-246x.2005.02783.x.

Barnes, P. M. Postglacial (after 20 ka) dextral slip rate of the offshore Alpine fault, New Zealand. *Geology*, 37(1):3–6, Jan. 2009. doi: 10.1130/g24764a.1.

Barrell, D. General distribution and characteristics of active faults and folds in the Waimate District and Waitaki Distict, South Canterbury and North Otago,. *GNS Science Consultancy Report 2015/166*, pages 1–124, 2016. https://www.orc.govt.nz/media/3965/general-distribution-and-characteristics-of-active-faults-and-folds-in-the-waimate-district-and-waitaki-district-south-canterbury-and-north-otago.pdf.

Barrell, D. General distribution and characteristics of active faults and folds in the Queenstown Lakes and Central Otago districts, Otago. *GNS Science, Consultancy Report 2018/207*, pages 1–99, 2019. https://www.orc.govt.nz/media/6621/gns_cr2018-207_queenstown-lakes-and-central-otago_active-faults.pdf.

Barrell, D. General distributions and characteristics of active faults and folds in the Clutha and Dunedin City districts, Otago. *GNS Science, Consultancy Report 2020/88*, pages 1–71, 2021. https://www.orc.govt.nz/media/10002/active-faults-folds-in-the-clutha-and-dunedin-city-districts-otago-2021.pdf.

Barrell, D. J. A., Read, S. A. L., Van Dissen, R. J., Macfarlane, D. F., Walker, J., and Rieser, U. Aviemore: A dam of two halves. In *Joint annual conference of the Geological Society of New Zealand and the New Zealand Geophysical Society: Field trip guides B*, volume 128. Geol. Soc. New Zeal. Misc. Publ, 2009.

Barth, N., Kulhanek, D., Beu, A., Murray-Wallace, C., Hayward, B., Mildenhall, D., and Lee, D. New c. 270 kyr strike-slip and uplift rates for the southern Alpine Fault and implications for the New Zealand plate boundary. *Journal of Structural Geology*, 64: 39–52, July 2014. doi: 10.1016/j.jsg.2013.08.009.

Barton, C. A. and Zoback, M. D. Self-similar distribution and properties of macroscopic fractures at depth in crystalline rock in the Cajon Pass Scientific Drill Hole. *Journal of Geophysical Research: Solid Earth*, 97(B4):5181–5200, Apr. 1992. doi: 10.1029/91jb01674.

Boese, C. M., Townend, J., Smith, E., and Stern, T. Microseismicity and stress in the vicinity of the Alpine Fault, central Southern Alps, New Zealand. *Journal of Geophysical Research: Solid Earth*, 117(B2), Feb. 2012. doi: 10.1029/2011jb008460.

Bott, M. H. P. The Mechanics of Oblique Slip Faulting. *Geological Magazine*, 96(2):109–117, Apr. 1959. doi: 10.1017/s0016756800059987.

Browne, G., Field, B., Barrell, D., Jongens, R., Bassett, K., and Wood, R. The geological setting of the Darfield and Christchurch earthquakes. *New Zealand Journal of Geology and Geophysics*, 55(3):193–197, Aug. 2012. doi: 10.1080/00288306.2012.682654.

Cox, S. C. and Sutherland, R. *Regional geological framework of South Island, New Zealand, and its significance for understanding the active plate boundary*, page 19–46. American Geophysical Union, 2007. doi: 10.1029/175gm03.

Cox, S. C., Stirling, M. W., Herman, F., Gerstenberger, M., and Ristau, J. Potentially active faults in the rapidly eroding landscape adjacent to the Alpine Fault, central Southern Alps, New Zealand. *Tectonics*, 31(2), Apr. 2012. doi: 10.1029/2011tc003038.

Craw, D., Campbell, C., and Waters, J. M. Miocene-Holocene river drainage evolution in Southland, New Zealand, deduced from fish genetics, detrital gold and geology. *New Zealand Journal of Geology and Geophysics*, 67(1):146–159, Sept. 2022. doi: 10.1080/00288306.2022.2121289.

Célérier, B. Seeking Anderson's faulting in seismicity: A centennial celebration. *Reviews of Geophysics*, 46(4), Oct. 2008. doi: 10.1029/2007rg000240.

DeMets, C., Gordon, R. G., and Argus, D. F. Geologically current plate motions. *Geophysical Journal International*, 181(1):1–80, Apr. 2010. doi: 10.1111/j.1365-246x.2009.04491.x.

Denys, P., Pearson, C., Norris, R., and Denham, M. A geodetic study of Otago: results of the central Otago deformation network 2004–2014. *New Zealand Journal of Geology and Geophysics*, 59 (1):147–156, Jan. 2016. doi: 10.1080/00288306.2015.1134592.

Dewey, J. F., Holdsworth, R. E., and Strachan, R. A. Transpression and transtension zones. *Geological Society, London, Special Publications*, 135(1):1–14, Jan. 1998. doi: 10.1144/gsl.sp.1998.135.01.01.

Eberhart-Phillips, D. and Reyners, M. Catalogue of 2001–2011 New Zealand earthquakes relocated with 3-D seismic velocity model and comparison to 2019–2020 auto-detected earthquakes in the sparsely instrumented southern South Island. *New Zealand Journal of Geology and Geophysics*, 66(4):646–653, 2023. doi: 10.1080/00288306.2022.2089171.

Eberhart-Phillips, D., Reyners, M., Upton, P., and Gubbins, D. Insights into the structure and tectonic history of the southern South Island, New Zealand, from the 3-D distribution of P- and S-wave attenuation. *Geophysical Journal International*, 214(2): 1479–1505, May 2018. doi: 10.1093/gji/ggy194.

Eberhart-Phillips, D., Bannister, S., Reyners, M., and Bourguignon, S. New Zealand Wide model 2.3 seismic velocity model for New Zealand, 2022a. doi: 10.5281/ZENODO.6568301.

Eberhart-Phillips, D., Upton, P., Reyners, M., Barrell, D. J., Fry, B., Bourguignon, S., and Warren-Smith, E. The Influence of Basement Terranes on Tectonic Deformation: Joint Earthquake Travel-Time and Ambient Noise Tomography of the Southern South Island, New Zealand. *Tectonics*, 41(4):e2021TC007006, 2022b. doi: 10.1029/2021TC007006.

Eberhart-Phillips, D., Bourguignon, S., and Salichon, J. Lithospheric structure of the Fiordland plutonic block controls deformation in the subduction transition along southwestern New Zealand,. In *AGU Fall Meeting Abstracts, S32c-06*, 2023.

Eberhart-Phillips, D., Thurber, C., Rietbrock, A., Fry, B., Reyners, M., and Lanza, F. Simul2023: a flexible program for inversion of earthquake data for 3-D velocity and hypocenters or 3-D Q, 2024. doi: 10.5281/ZENODO.10695070.

Ellis, S., Williams, C., Ristau, J., Reyners, M., Eberhart-Phillips, D., and Wallace, L. Calculating regional stresses for northern Canterbury: the effect of the 2010 Darfield earthquake. *New Zealand Journal of Geology and Geophysics*, 59(1):202–212, Jan. 2016. doi: 10.1080/00288306.2015.1123740.

Enlow, R. L. and Koons, P. O. Critical wedges in three dimensions: Analytical expressions from Mohr-Coulomb constrained perturbation analysis. *Journal of Geophysical Research: Solid Earth*, 103(B3):4897–4914, Mar. 1998. doi: 10.1029/97jb03209.

Faulkner, D. R., Mitchell, T. M., Healy, D., and Heap, M. J. Slip on "weak" faults by the rotation of regional stress in the fracture damage zone. *Nature*, 444(7121):922–925, Dec. 2006. doi: 10.1038/nature05353.

Ferrill, D. A., Smart, K. J., and Morris, A. P. Fault failure modes, deformation mechanisms, dilation tendency, slip tendency, and conduits v. seals. *Geological Society, London, Special Publications*, 496(1):75–98, Dec. 2019. doi: 10.1144/sp496-2019-7.

Forsyth, P. Geology of the Waitaki area. Technical report, Institute of Geological and Nuclear Sciences 1:250,000 geology map 19,

Lower Hutt (NZ), 2002.

Fossen, H. *Fault classification, fault growth and displacement*, page 119–147. Elsevier, 2020. doi: 10.1016/b978-0-444-64134-2.00007-9.

Gorman, A., Hill, M., Orpin, A., Koons, P., Norris, R., Landis, C., Allan, T., Johnstone, T., Gray, F., Wilson, D., and Osterberg, E. Quaternary shelf structures SE of the South Island, imaged by high-resolution seismic profiling. *New Zealand Journal of Geology and Geophysics*, 56(2):68–82, June 2013. doi: 10.1080/00288306.2013.772906.

Griffin, J. D., Stirling, M. W., Wilcken, K. M., and Barrell, D. J. A. Late Quaternary Slip Rates for the Hyde and Dunstan Faults, Southern New Zealand: Implications for Strain Migration in a Slowly Deforming Continental Plate Margin. *Tectonics*, 41(9), Sept. 2022. doi: 10.1029/2022tc007250.

Gudmundsson, A., Simmenes, T. H., Larsen, B., and Philipp, S. L. Effects of internal structure and local stresses on fracture propagation, deflection, and arrest in fault zones. *Journal of Structural Geology*, 32(11):1643–1655, Nov. 2010. doi: 10.1016/j.jsg.2009.08.013.

Haines, A. J. and Wallace, L. M. New Zealand-Wide Geodetic Strain Rates Using a Physics-Based Approach. *Geophysical Research Letters*, 47(1), Jan. 2020. doi: 10.1029/2019gl084606.

Hardebeck, J. L. Using S/P Amplitude Ratios to Constrain the Focal Mechanisms of Small Earthquakes. *Bulletin of the Seismological Society of America*, 93(6):2434–2444, Dec. 2003. doi: 10.1785/0120020236.

Hardebeck, J. L. and Hauksson, E. Crustal stress field in southern California and its implications for fault mechanics. *Journal of Geophysical Research: Solid Earth*, 106(B10):21859–21882, Oct. 2001. doi: 10.1029/2001jb000292.

Hardebeck, J. L. and Shearer, P. M. A New Method for Determining First-Motion Focal Mechanisms. *Bulletin of the Seismological Society of America*, 92(6):2264–2276, Aug. 2002. doi: 10.1785/0120010200.

Hartigan, J. A. and Wong, M. A. Algorithm AS 136: A K-Means Clustering Algorithm. *Applied Statistics*, 28(1):100, 1979. doi: 10.2307/2346830.

Heidbach, O., Rajabi, M., Cui, X., Fuchs, K., Müller, B., Reinecker, J., Reiter, K., Tingay, M., Wenzel, F., Xie, F., Ziegler, M. O., Zoback, M.-L., and Zoback, M. The World Stress Map database release 2016: Crustal stress pattern across scales. *Tectonophysics*, 744: 484–498, Oct. 2018. doi: 10.1016/j.tecto.2018.07.007.

Holbek, S. C., Frank, M., Scott, J. M., Smith, S. A. F., le Roux, P. J., Waight, T. E., Van Hale, R., Reid, M. R., and Stirling, C. H. Structural Controls on Shallow Cenozoic Fluid Flow in the Otago Schist, New Zealand. *Geofluids*, 2020:1–25, Aug. 2020. doi: 10.1155/2020/9647197.

Holt, R., Savage, M., Townend, J., Syracuse, E., and Thurber, C. Crustal stress and fault strength in the Canterbury Plains, New Zealand. *Earth and Planetary Science Letters*, 383:173–181, Dec. 2013. doi: 10.1016/j.epsl.2013.09.041.

Hull, A. G. and Stirling, M. W. Re-evaluation of late Quaternary displacement along the Old Man Fault Zone at Gorge Creek, Central Otago, New Zealand. *New Zealand Journal of Geology and Geophysics*, 35(2):259–262, June 1992. doi: 10.1080/00288306.1992.9514519.

Jones, R. R. and Tanner, P. G. Strain partitioning in transpression zones. *Journal of Structural Geology*, 17(6), 1995. doi: 10.1016/0191-8141(94)00102-6.

Kilb, D. and Hardebeck, J. L. Fault Parameter Constraints Using Relocated Earthquakes: A Validation of First-Motion Focal-Mechanism Data. *Bulletin of the Seismological Society of America*, 96(3):1140–1158, June 2006. doi: 10.1785/0120040239.

Kim, N., Park, S.-I., Cho, C. S., Cheon, Y., and Peace, A. L. Neotectonic transpressional intraplate deformation in eastern Eurasia: Insights from active fault systems in the southeastern Korean Peninsula. *Geoscience Frontiers*, 14(4):101559, July 2023. doi: 10.1016/j.gsf.2023.101559.

Koons, P. O. Three-dimensional critical wedges: Tectonics and topography in oblique collisional orogens. *Journal of Geophysical Research: Solid Earth*, 99(B6):12301–12315, June 1994. doi: 10.1029/94jb00611.

Lanari, R., Faccenna, C., Fellin, M., Essaifi, A., Nahid, A., Medina, F., and Youbi, N. Tectonic Evolution of the Western High Atlas of Morocco: Oblique Convergence, Reactivation, and Transpression. *Tectonics*, 39(3), Mar. 2020. doi: 10.1029/2019tc005563.

Landis, C. A., Campbell, H. J., Aslund, T., Cawood, P. A., Douglas, A., Kimbrough, D. L., Pillai, D. D. L., Raine, J. I., and Willsman, A. Permian-Jurassic strata at Productus Creek, Southland, New Zealand: Implications for terrane dynamics of the eastern Gondwanaland margin. *New Zealand Journal of Geology and Geophysics*, 42(2):255–278, June 1999. doi: 10.1080/00288306.1999.9514844.

Leitner, B., Eberhart-Phillips, D., Anderson, H., and Nabelek, J. L. A focused look at the Alpine fault, New Zealand: Seismicity, focal mechanisms, and stress observations. *Journal of Geophysical Research: Solid Earth*, 106(B2):2193–2220, 2001. doi: https://-doi.org/10.1029/2000JB900303.

Lettis, W. R. and Hanson, K. L. Crustal strain partitioning: Implications for seismic-hazard assessment in western California. *Geology*, 19(6):559, 1991. doi: 10.1130/0091-7613(1991)019<0559:cspifs>2.3.co;2.

Lisle, R. J., Orife, T. O., Arlegui, L., Liesa, C., and Srivastava, D. C. Favoured states of palaeostress in the Earth's crust: evidence from fault-slip data. *Journal of Structural Geology*, 28(6): 1051–1066, June 2006. doi: 10.1016/j.jsg.2006.03.012.

Litchfield, N. J. The Titri Fault System: Quaternary-active faults near the leading edge of the Otago reverse fault province. *New Zealand Journal of Geology and Geophysics*, 44(4):517–534, Dec. 2001. doi: 10.1080/00288306.2001.9514953.

Lund, B. and Slunga, R. Stress tensor inversion using detailed microearthquake information and stability constraints: Application to Ölfus in southwest Iceland. *Journal of Geophysical Research: Solid Earth*, 104(B7):14947–14964, July 1999. doi: 10.1029/1999jb900111.

López, A. Andersonian and Coulomb stresses in Central Costa Rica and its fault slip tendency potential: new insights into their associated seismic hazard. *Geological Society, London, Special Publications*, 367(1):19–38, Aug. 2012. doi: 10.1144/sp367.3.

Martínez-Garzón, P., Ben-Zion, Y., Abolfathian, N., Kwiatek, G., and Bohnhoff, M. A refined methodology for stress inversions of earthquake focal mechanisms. *Journal of Geophysical Research: Solid Earth*, 121(12):8666–8687, Dec. 2016. doi: 10.1002/2016jb013493.

Matsuno, M., Tagami, A., Okada, T., Matsumoto, S., Kawamura, Y., Iio, Y., Sato, T., Nakayama, T., Hirahara, S., Bannister, S., Ristau, J., Savage, M. K., Thurber, C. H., and Sibson, R. H. Spatial and temporal stress field changes in the focal area of the 2016 Kaikōura earthquake, New Zealand: A multi-fault process interpretation. *Tectonophysics*, 835:229390, July 2022. doi: 10.1016/j.tecto.2022.229390.

McCaffrey, R. The Tectonic Framework of the Sumatran Subduction Zone. *Annual Review of Earth and Planetary Sciences*, 37(1): 345–366, May 2009. doi: 10.1146/annurev.earth.031208.100212.

Mercier, J., Armijo, R., Tapponnier, P., Carey-Gailhardis, E., and Lin, H. T. Change from Late Tertiary compression to Quaternary ex-

tension in southern Tibet during the India-Asia Collision. *Tectonics*, 6(3):275–304, June 1987. doi: 10.1029/tc006i003p00275.

Meyer, A. F. T., Stirling, M. W., Griffin, J. D., Tarling, M. S., Stirling, T. W., and Thomsen, J. M. Paleoseismology of the Long Valley Fault, Central Otago, New Zealand. *New Zealand Journal of Geology and Geophysics*, 68(4):889–896, July 2025. doi: 10.1080/00288306.2025.2519711.

Michael, A. J. Determination of stress from slip data: Faults and folds. *Journal of Geophysical Research: Solid Earth*, 89(B13): 11517–11526, Dec. 1984. doi: 10.1029/jb089ib13p11517.

Michael, A. J. Use of focal mechanisms to determine stress: A control study. *Journal of Geophysical Research: Solid Earth*, 92(B1): 357–368, Jan. 1987. doi: 10.1029/jb092ib01p00357.

Michailos, K., Warren-Smith, E., Savage, M. K., and Townend, J. Detailed spatiotemporal analysis of the tectonic stress regime near the central Alpine Fault, New Zealand. *Tectonophysics*, 775: 228205, Jan. 2020. doi: 10.1016/j.tecto.2019.228205.

Miller, D. D. Distributed shear, rotation, and partitioned strain along the San Andreas fault, central California. *Geology*, 26(10):867, 1998. doi: 10.1130/0091-7613(1998)026<0867:dsraps>2.3.co;2.

Morley, C. Stress re-orientation along zones of weak fabrics in rifts: An explanation for pure extension in 'oblique' rift segments? *Earth and Planetary Science Letters*, 297(3–4):667–673, Sept. 2010. doi: 10.1016/j.epsl.2010.07.022.

Morris, A., Ferrill, D. A., and Brent Henderson, D. Slip-tendency analysis and fault reactivation. *Geology*, 24(3):275, 1996. doi: 10.1130/0091-7613(1996)024<0275:staafr>2.3.co;2.

Mortimer, N., Lee, J., and Stockli, D. F. Terrane and core complex architecture of the Otago Schist in the Dunstan and Cairnmuir Mountains, New Zealand, from U-Pb and (U-Th)/He zircon dating. *New Zealand Journal of Geology and Geophysics*, 67(2): 195–208, Feb. 2023. doi: 10.1080/00288306.2023.2176892.

Mount, V. S. and Suppe, J. State of stress near the San Andreas fault: Implications for wrench tectonics'. *Geology*, 15:1143–1146, 1988. doi: 10.1130/0091-7613(1988)016<1151:COSOSN>2.3.CO;2.

Norris, R., Koons, P., and Cooper, A. The obliquely-convergent plate boundary in the South Island of New Zealand: implications for ancient collision zones. *Journal of Structural Geology*, 12(5–6):715–725, Jan. 1990. doi: 10.1016/0191-8141(90)90084-c.

Norris, R. J. Strain localisation within ductile shear zones beneath active faults: The Alpine Fault contrasted with the adjacent Otago fault system, New Zealand. *Earth, Planets and Space*, 56(12):1095–1101, June 2014. doi: 10.1186/bf03353328.

Norris, R. J. and Cooper, A. F. Late Quaternary slip rates and slip partitioning on the Alpine Fault, New Zealand. *Journal of Structural Geology*, 23(2–3):507–520, Feb. 2001. doi: 10.1016/s0191-8141(00)00122-x.

Reyners, M. Otago temporary broadband network. International Federation of Digital Seismograph Networks, 2014. doi: 10.7914/SN/6K_2014.

Reyners, M., Eberhart-Phillips, D., and Bannister, S. Tracking repeated subduction of the Hikurangi Plateau beneath New Zealand. *Earth and Planetary Science Letters*, 311(1–2):165–171, Nov. 2011. doi: 10.1016/j.epsl.2011.09.011.

Reyners, M., Eberhart-Phillips, D., Upton, P., and Gubbins, D. Three-dimensional imaging of impact of a large igneous province with a subduction zone. *Earth and Planetary Science Letters*, 460:143–151, Feb. 2017. doi: 10.1016/j.epsl.2016.12.025.

Ristau, J. Update of Regional Moment Tensor Analysis for Earthquakes in New Zealand and Adjacent Offshore Regions. *Bulletin of the Seismological Society of America*, 103(4):2520–2533, July 2013. doi: 10.1785/0120120339.

Robinson, R. and McGinty, P. J. The enigma of the Arthur's Pass, New Zealand, earthquake: 2. The aftershock distribution and its relation to regional and induced stress fields. *Journal of Geophysical Research: Solid Earth*, 105(B7):16139–16150, July 2000. doi: 10.1029/2000jb900012.

Rousseeuw, P. J. Silhouettes: A graphical aid to the interpretation and validation of cluster analysis. *Journal of Computational and Applied Mathematics*, 20:53–65, Nov. 1987. doi: 10.1016/0377-0427(87)90125-7.

Sanderson, D. J. and Marchini, W. Transpression. *Journal of Structural Geology*, 6(5):449–458, Jan. 1984. doi: 10.1016/0191-8141(84)90058-0.

Scholz, C. H. *The mechanics of earthquakes and faulting*. Cambridge university press, third edit edition, 2019.

Scholz, C. H. and Choi, E. What comes first: The fault or the ductile shear zone? *Earth and Planetary Science Letters*, 577:117273, Jan. 2022. doi: 10.1016/j.epsl.2021.117273.

Schütt, J. M. and Whipp, D. M. Controls on Continental Strain Partitioning Above an Oblique Subduction Zone, Northern Andes. *Tectonics*, 39(4):1–21, 2020. doi: 10.1029/2019TC005886.

Seebeck, H., Van Dissen, R. J., Litchfield, N. J., Barnes, P., Nicol, A., Langridge, R., Barrell, D., Villamor, P., Ellis, S., Rattenbury, M., Bannister, S., Gerstenberger, M., Ghisetti, F., Sutherland, R., Fraser, J., Nodder, S., Stirling, M., Humphrey, J., Bland, K., Howell, A., Mountjoy, J. J., Moon, V., Stahl, T., Spinardi, F., Townsend, D., Clark, K., Hamling, I., Cox, S., de Lange, W., Wopereis, P., Johnston, M., Morgenstern, R., Coffey, G., Eccles, J., Little, T., Fry, B., Griffin, J., Mortimer, N., Alcaraz, S., Massiot, C., Rowland, J., Muirhead, J., Upton, P., Hirschberg, H., and Lee, J. New Zealand Community Fault Model - version 1.0. Technical report, 2022. doi: 10.21420/GA7S-BS61.

Seebeck, H., Dissen, R. V., Litchfield, N., Barnes, P. M., Nicol, A., Langridge, R., Barrell, D. J. A., Villamor, P., Ellis, S., Rattenbury, M., Bannister, S., Gerstenberger, M., Ghisetti, F., Sutherland, R., Hirschberg, H., Fraser, J., Nodder, S. D., Stirling, M., Humphrey, J., Bland, K. J., Howell, A., Mountjoy, J., Moon, V., Stahl, T., Spinardi, F., Townsend, D., Clark, K., Hamling, I., Cox, S., de Lange, W., Wopereis, P., Johnston, M., Morgenstern, R., Coffey, G., Eccles, J. D., Little, T., Fry, B., Griffin, J., Townend, J., Mortimer, N., Alcaraz, S., Massiot, C., Rowland, J. V., Muirhead, J., Upton, P., and Lee, J. The New Zealand Community Fault Model – version 1.0: an improved geological foundation for seismic hazard modelling. *New Zealand Journal of Geology and Geophysics*, 67(2):209–229, 2024. doi: 10.1080/00288306.2023.2181362.

Sibson, R. H. Crustal stress, faulting and fluid flow. *Geological Society, London, Special Publications*, 78(1):69–84, Jan. 1994. doi: 10.1144/gsl.sp.1994.078.01.07.

Sibson, R. H., Ghisetti, F. C., and Crookbain, R. A. Andersonian wrench faulting in a regional stress field during the 2010–2011 Canterbury, New Zealand, earthquake sequence. *Geological Society, London, Special Publications*, 367(1):7–18, Aug. 2012. doi: 10.1144/sp367.2.

Smith, S., Tesei, T., Scott, J., and Collettini, C. Reactivation of normal faults as high-angle reverse faults due to low frictional strength: Experimental data from the Moonlight Fault Zone, New Zealand. *Journal of Structural Geology*, 105:34–43, Dec. 2017. doi: 10.1016/j.jsg.2017.10.009.

Tamas, A., Holdsworth, R. E., Underhill, J. R., Tamas, D. M., Dempsey, E. D., Hardman, K., Bird, A., McCarthy, D., McCaffrey, K. J., and Selby, D. New onshore insights into the role of struc-

tural inheritance during Mesozoic opening of the Inner Moray Firth Basin, Scotland. *Journal of the Geological Society*, 179(2), Nov. 2021. doi: 10.1144/jgs2021-066.

Taylor-Silva, B. I., Stirling, M. W., Litchfield, N. J., Griffin, J. D., van den Berg, E. J., and Wang, N. Paleoseismology of the Akatore Fault, Otago, New Zealand. *New Zealand Journal of Geology and Geophysics*, 63(2):151–167, 2020. doi: 10.1080/00288306.2019.1645706.

Teyssier, C., Tikoff, B., and Markley, M. Oblique plate motion and continental tectonics. *Geology*, 23(5):447, 1995. doi: 10.1130/0091-7613(1995)023<0447:opmact>2.3.co;2.

Thingbaijam, K. K. S., Rattenbury, M. S., Van Dissen, R. J., Gerstenberger, M. C., Ristau, J., and Fitzenz, D. D. Characterization of Focal Mechanisms for Upper Crustal Distributed Seismicity in Aotearoa New Zealand. *Seismological Research Letters*, 95(1): 150–158, Oct. 2023. doi: 10.1785/0220230196.

Thurber, C. and Eberhart-Phillips, D. Local earthquake tomography with flexible gridding. *Computers & Geosciences*, 25(7): 809–818, Aug. 1999. doi: 10.1016/s0098-3004(99)00007-2.

Townend, J., Sherburn, S., Arnold, R., Boese, C., and Woods, L. Three-dimensional variations in present-day tectonic stress along the Australia–Pacific plate boundary in New Zealand. *Earth and Planetary Science Letters*, 353–354:47–59, Nov. 2012. doi: 10.1016/j.epsl.2012.08.003.

Turnbull, I. M. Geology of the Wakatipu area. Technical report, Institute of Geological and Nuclear Sciences, Lower Hutt (NZ), 2000.

Turnbull, I. M. and Allibone, A. H. Geology of the Murihiku area. Technical report, Institute of Geological and Nuclear Sciences, Lower Hutt (NZ), 2003.

Turnbull, I. M., Craw, D., and Norris, R. J. Pre-Miocene and post-Miocene deformation in the Bannockburn basin, Central Otago, New Zealand. *New Zealand Journal of Geology and Geophysics*, 36(1):107–115, Jan. 1993. doi: 10.1080/00288306.1993.9514558.

Twiss, R. J. and Unruh, J. R. Analysis of fault slip inversions: Do they constrain stress or strain rate? *Journal of Geophysical Research: Solid Earth*, 103(B6):12205–12222, June 1998. doi: 10.1029/98jb00612.

Upton, P., Koons, P. O., Craw, D., Henderson, C. M., and Enlow, R. Along-strike differences in the Southern Alps of New Zealand: Consequences of inherited variation in rheology. *Tectonics*, 28 (2), Mar. 2009. doi: 10.1029/2008tc002353.

Upton, P., Craw, D., and Walcott, R. Far-Field Deformation Resulting from Rheologic Differences Interacting with Tectonic Stresses: An Example from the Pacific/Australian Plate Boundary in Southern New Zealand. *Geosciences*, 4(3):93–113, July 2014. doi: 10.3390/geosciences4030093.

van den Berg, E. J., Williams, J. N., Stirling, M. W., Barrell, D. J. A., Griffin, J. D., Litchfield, N. J., and Wang, N. Late Quaternary activity of the NW Cardrona Fault, Otago, New Zealand. *New Zealand Journal of Geology and Geophysics*, 68(1):151–171, Jan. 2024. doi: 10.1080/00288306.2023.2297962.

Vavryčuk, V. Iterative joint inversion for stress and fault orientations from focal mechanisms. *Geophysical Journal International*, 199(1):69–77, July 2014. doi: 10.1093/gji/ggu224.

Vollmer, F. W. C program for automatic contouring of spherical orientation data using a modified Kamb method. *Computers & Geosciences*, 21(1):31–49, Feb. 1995. doi: 10.1016/0098-3004(94)00058-3.

Waldien, T. S., Roeske, S. M., Chatterjee, R., O'Sullivan, P. B., and Stockli, D. F. Suture Reactivation, Slip Partitioning, and a Protracted Strike-Slip Rate Gradient in the Denali Fault System, Southern Alaska, USA. *Tectonics*, 42(9), Sept. 2023. doi: 10.1029/2022tc007654.

Wallace, R. E. Geometry of Shearing Stress and Relation to Faulting. *The Journal of Geology*, 59(2):118–130, Mar. 1951. doi: 10.1086/625831.

Warren-Smith, E., Jacobs, K., Rollins, C., Chamberlain, C. J., Eberhart-Phillips, D., and Williams, C. A quantitative assessment of GeoNet earthquake location quality in Aotearoa New Zealand. *New Zealand Journal of Geology and Geophysics*, 68 (5):941–954, Dec. 2024. doi: 10.1080/00288306.2024.2421309.

Warren-Smith, E., Lamb, S., and Stern, T. A. Stress field and kinematics for diffuse microseismicity in a zone of continental transpression, South Island, New Zealand. *Journal of Geophysical Research: Solid Earth*, 122(4):2798–2811, Apr. 2017a. doi: 10.1002/2017jb013942.

Warren-Smith, E., Lamb, S., Stern, T. A., and Smith, E. Microseismicity in Southern South Island, New Zealand: Implications for the Mechanism of Crustal Deformation Adjacent to a Major Continental Transform. *Journal of Geophysical Research: Solid Earth*, 122(11):9208–9227, Nov. 2017b. doi: 10.1002/2017jb014732.

Warren-Smith, E., Townend, J., Chamberlain, C. J., Boulton, C., and Michailos, K. Heterogeneity in Microseismicity and Stress Near Rupture-Limiting Section Boundaries Along the Late-Interseismic Alpine Fault. *Journal of Geophysical Research: Solid Earth*, 127(10), Oct. 2022. doi: 10.1029/2022jb025219.

Webb, T. H. and Anderson, H. Focal mechanisms of large earthquakes in the North Island of New Zealand: slip partitioning at an oblique active margin. *Geophysical Journal International*, 134(1):40–86, July 1998. doi: 10.1046/j.1365-246x.1998.00531.x.

Williams, J., Stirling, M., Langridge, R., Niroula, G., Vause, A., Stewart, J., Nicol, A., and Wang, N. Along-strike extent of earthquakes on multi-segment reverse faults; insights from the Nevis-Cardrona Fault, Aotearoa New Zealand. *Seismica*, 3(2), Oct. 2024. doi: 10.26443/seismica.v3i2.1310.

Williams, J., Eberhart-Phillips, D., Bourguignon, S., Stirling, M., Reyners, M., and Upton, P. Supplementary files to "Focal mechanisms in the southeastern South Island of Aotearoa New Zealand indicate scale-dependent partitioning of transpressional strain". Technical report, Sept. 2025a. doi: 10.5281/zenodo.17228270.

Williams, J. N., Fagereng, A., Wedmore, L. N. J., Biggs, J., Mphepo, F., Dulanya, Z., Mdala, H., and Blenkinsop, T. How Do Variably Striking Faults Reactivate During Rifting? Insights From Southern Malawi. *Geochemistry, Geophysics, Geosystems*, 20(7): 3588–3607, July 2019. doi: 10.1029/2019gc008219.

Williams, J. N., Eberhart-Phillips, D., Bourguignon, S., and Stirling, M. Southland Otago Seismic Array. International Federation of Digital Seismograph Networks, 2022. doi: 10.7914/JR68-QQ17.

Williams, J. N., Eberhart-Phillips, D., Bourguignon, S., Stirling, M. W., and Oliver, W. Deep and Clustered Microseismicity at the Edge of Southern New Zealand's Transpressive Plate Boundary. *Journal of Geophysical Research: Solid Earth*, 130(5): e2024JB030371, 2025b. doi: 10.1029/2024JB030371.

Williams, J. N., Stirling, M. W., Howell, A., Niroula, G. P., DiCaprio, C. J., McGrath, J., Gerstenberger, M. C., Coffey, G. L., Griffin, J. D., Van Dissen, R., Penney, C., and Chamberlain, C. Evaluating and Comparing Seismicity Rate Models in the Low-Strain-Rate Otago Region, Aotearoa, New Zealand. *Bulletin of the Seismological Society of America*, 115(5):2237–2262, 07 2025c. doi: 10.1785/0120240277.

Yang, W., Hauksson, E., and Shearer, P. M. Computing a Large Refined Catalog of Focal Mechanisms for Southern California

(1981-2010): Temporal Stability of the Style of Faulting. *Bulletin of the Seismological Society of America*, 102(3):1179–1194, June 2012. doi: 10.1785/0120110311.

Yukutake, Y., Takeda, T., and Yoshida, A. The applicability of frictional reactivation theory to active faults in Japan based on slip tendency analysis. *Earth and Planetary Science Letters*, 411: 188–198, Feb. 2015. doi: 10.1016/j.epsl.2014.12.005.

Zhang, Y., Levandowski, W., Powell, C., and Langston, C. A. Transpressive Stress Throughout the New Madrid Seismic Zone, With Second-Order Variations: Evidence From Focal Mechanism Inversions. *Tectonics*, 44(5), May 2025. doi: 10.1029/2024tc008447.

Ziegler, M. O., Seithel, R., Niederhuber, T., Heidbach, O., Kohl, T., Müller, B., Rajabi, M., Reiter, K., and Röckel, L. Stress state at faults: the influence of rock stiffness contrast, stress orientation, and ratio. *Solid Earth*, 15(8):1047–1063, Aug. 2024. doi: 10.5194/se-15-1047-2024.

The article *Focal mechanisms in the southeastern South Island of Aotearoa New Zealand indicate scale-dependent partitioning of transpressional strain* © 2026 by Jack N. Williams is licensed under CC BY 4.0.